DYNAMIC MODELING AND FIELD TESTING OF STEEL RAILWAY BRIDGES

By

PENG LOU

A thesis submitted to the

Graduate School-New Brunswick

Rutgers, The State University of New Jersey

in partial fulfillment of the requirements

for the degree of

Master of Science

Graduate Program in Civil and Environmental Engineering

written under the direction of

Dr. Hani H. Nassif

and approved by

_____

_____

_____

New Brunswick, New Jersey

May 2012

ABSTRACT OF THE THESIS

DYNAMIC MODELING AND FIELD TESTING OF STEEL RAILWAY BRIDGES

By PENG LOU

Thesis Director:
Dr. Hani H. Nassif

In United State, there are a lot of steel railway bridges with non-ballast tracks, which have short and simply supported spans. The majority of similar bridges on the passenger rail systems were built prior to World War II. In New Jersey, freight railcars often utilize a portion of passenger rail systems to complete their trips. Recent increases in railcar weight limits from 263,000 lb to 286,000 lb raised concerns about the passenger rail systems since these bridges were not designed according to the increased railcar weight. Also, the cost to build and maintain new bridges is extremely high. Therefore, impact of the increased railcar weight on those bridges need to be evaluated first to allow the use of passenger lines for the freight travels. The research approach adopted is aiming at evaluating current load-carrying capacity of various types of bridges to provide recommendations for dynamic impact. The impact factor equations specified in AREMA Specifications were based on field tests prior to 1960s. It is important to validate and evaluate the impact factor equation from recent field tests.

In this thesis, a 2D dynamic model of train-bridge interaction system was developed. Steel bridge is simulated as a Bernoulli-Euler beam and moving train is modeled as rigid-body. Field measurement was conducted to obtain the strain, deflection, and velocity response of bridge girders under moving trains via wireless Structural Testing System (STS) and non-contact Laser Doppler Vibrometer (LDV). The validity of the presented model was confirmed through comparison with the measured structural response. Impact factor (IF) was then obtained from the validated dynamic model. Train speed, train type, bridge span length, and girder stiffness were considered as the main parameters affecting the IF. The results of this study show that the present AREMA Specifications has a tendency to overestimate the IF at speeds lower than 60 mph for steel bridges.

ACKNOWLEDGEMENTS

I would like start by thanking Dr. Hani H. Nassif for his continuous support throughout my study at Rutgers. It was a great honor for me to have him as an advisor and a friend who was always there for me in any imaginable way.

I would also like to thank Dr. Kaan Ozbay and Dr. Wang Hao for being in my thesis committee and their invaluable advice.

I would like to thank Dr. Yingjie Wang and Dan Su for helping me to get started with this research in the lab and for being available whenever I needed them.

I would like to thank my father, mother and all my family members who always support my decisions and inspire me with their success, life experiences, care and love. I would like to thank Giselle for sharing her experiences, for listening to my complaints and frustrations, and for believing in me.

I would like to thank Ye, Suhail, Ope, Khalid, Said, Zeeshan, Malek and all my friends in the lab that worked with me and eased my burden of tasks. This thesis wouldn't have been possible without you guys.

Special thanks also are to Gonca Unal, Gregory Wisniewski and Ryan Adams who have been great friends and colleagues throughout my studies here. Their creativity always showed me how to have fun in every tough situation. I will never forget them.

I would also like to thank my best friends Jie, Zikai, Xing, Cong, Xiang and Yuruo as well as all the other friends in my life who made me feel comfortable living here.

TABLE OF CONTENT

LIST OF FIGURES

xi

LIST OF TABLES

Chapter I

Introduction

1.1. Background

Nowadays, there is an increasing need in society to travel faster and further. This demand has to be covered with the implementation of efficient type of passenger transportation, which is able to cover the distances in a shorter time. The overall growth in the economy and population in the United States led to a significant expansion of railroad traffic levels by the late 1990s. In New Jersey, freight railcars utilize a portion of the passenger rail system. However, many of the bridges in the passenger rail line were built prior to World War II. Therefore, it is very important to evaluate the concerns about the condition of these bridges.

Normally when a low-speed load is applied on a structure, it is assumed that the acceleration of the mass of all elements and parts is equal to zero and also, that there is enough time so that equilibrium between external loads and internal elastic forces is achieved. In this case, static analysis is adequate for these structures. However, some loads create dynamic reactions in structures because of their rapid exertion, and common static analysis methods no longer acquire design requirements. Therefore, the dynamic effects of a moving train are important in the design and evaluation of the performance of

bridges especially for current high-speed railway lines being developed in many countries. This fact has caused some structural problems, which relate to both the design and the evaluation of bridges along the railways.

Normally, the dynamic effects seem to be caused by the interaction between a bridge and the vehicles that travel over the bridge. This interaction is a coupled, nonlinear dynamic problem. The dynamic interaction between a bridge and the vehicles is a special discipline within the wide range of area of structural dynamics. The vehicles considered may be generally those comprising the traffic flow of a highway bridge or particularly those that form a connected line of railroad cars. From the theoretical viewpoint, the two subsystems, i.e., the bridge and the vehicles can be simulated as two elastic structures, of which each is characterized by a frequency of vibration. The two subsystems interact with each other through the contact forces, i.e., the forces produced at the contact points between the wheel sets and rail surface of the railway bridge or pavement surface of the highway bridge. This is a nonlinear and time-dependent problem due to the fact that the contact forces may move from time to time and their magnitudes do not remain constant as a result of the relative movement of the two subsystems. The way by which the two subsystems interact with each other is determined primarily by the inherent frequencies of the two subsystems and the driving frequency of the moving vehicles. The interaction between the two subsystems is called vehicle–bridge interaction (VBI) [1].

From the aspect of structural dynamics, railway bridges are different from highway bridges because of the difference in the sources of excitation caused by the moving vehicles. For instance, the vehicles travelling over highway bridges are random. The

vehicles constituting the highway traffic may change in terms of the axle weight, axle interval, moving speed, and even the headway. However, a train moving over railway bridges can generally be regarded as a sequence of same vehicles in connection, plus one or two locomotives. Because of the repetitive nature of the wheel loads, a moving train usually contains some inherent frequencies, plus an excitation frequency related to the moving speed. If any of these frequencies coincide with any of the natural frequencies of vibrations of the bridge, the **resonance** phenomenon will induced on the bridge by the moving train. The response will be continuously amplified as more railroad cars pass the bridge. Under the condition of resonance, a great amplification in the bridge responses, as well as in the vehicle responses, can be expected, which is likely to affect the life time of the bridge and the riding quality of running vehicles. It is advisable that the phenomenon of resonance be circumvented from the onset in the design of railway bridges [1].

1.2. General studies on the Vehicle-Bridge Interaction (VBI)

The study of structural dynamic started in the middle of 19th century. On May 24 in 1847, the bridge over the River Dee in England collapsed. It happened again that a suspension bridge called Angers Bridge over the Maine River in Angers, France, collapsed on April 16 1850. Since then, many engineers and researchers at that time tried to explain this phenomenon with different theories. In 1851, R. Willis wrote some essays [2] demonstrating that a moving load over an elastic bar could cause deflection and stress larger than the same load in static. He developed a formula that increased the static response to cover the dynamic effects in a safe way [3]. The principal error of Willis'

theory was that he neglected the mass of beam that is compared with the mass of the load moving over the beam at a constant speed. This was the first attempt to get an impact coefficient from a historical viewpoint. Stokes [4] tried to develop Willis' work theoretically. His contribution mainly focused on the calculation of the forces exerted on bridges by moving engines. During the last 50 years of 19th century, Stokes investigated the reasons for failure of railway bridges.

In 1905, Krylov [5] proposed a complete solution to the dynamic problem of a moving load with a constant speed acting on a prismatic bar while in 1922 Timoshenko [6] solved the same problem but the force was a harmonic pulsating moving load. Both Krylov and Timoshenko considered that the mass of the moving load was negligible compared with the mass of the girder. This was different from the work done by Willis. Taking into account some new parameters, in 1934, Inglis [7] did another related work about the dynamic behavior of the railway bridges.

Ladislav Fryba also conducted an important research pertaining to the dynamic behavior of railway bridges. Fryba [8] studied the behavior of a simple supported beam under different types of moving loads including a moving multi-axle system and backed his analytical solution with real measurement data. Multi-axle vehicles are made up of a mechanical system with different degrees of freedom and include linear and non-linear springs and dampers. The inclusion of all of these parameters, besides other important parameters like span length, speed, axle distances, natural frequencies and permanent loads of the bridge represented one of the first theoretical models of a locomotive crossing over a beam with an elastic layer, irregularities and sleeper effects (Figure 1).
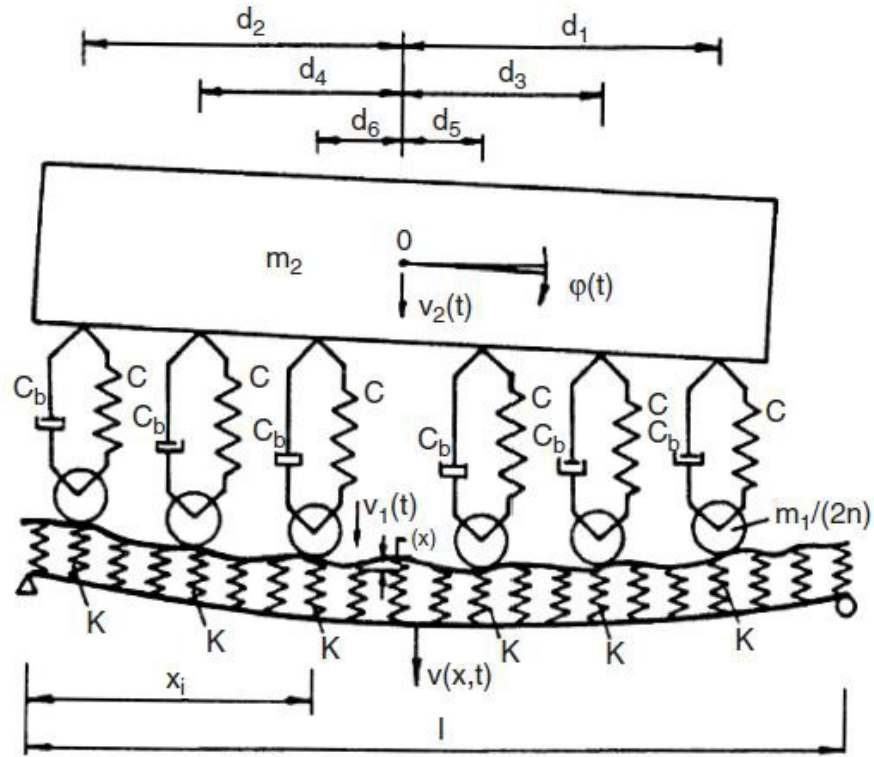
Figure 1. First theoretical model of a locomotive

In 2001, Fryba developed some simplified expressions to evaluate the critical speeds, the maximum deflection, bending moment, and vertical acceleration when a train runs over a bridge [9]. In order to obtain this, the author used a pointed load model. In the first part of the article, Fryba presented the classical development of the moving load problem, and consequently, he expanded these simple expressions to incorporate some criteria of interoperability in the railway network. In the article the measurements carried out for the TGV are compared with the simple expressions and the results were in agreement with each other, although ERRI D214 [10] indicates that these expressions usually give conservative estimations.

He Xia, from Beijing Jiaotong University, has been another of the most important investigators during last decade. His research focuses mainly on the dynamic behavior of high-speed railway bridges [11-16].

According to Xia and Zhang [11-16] the following simplifications are assumed for the majority of the vehicle models:

1. The train runs on the bridge at a constant speed.

2. The car body, bogies and wheel-sets of the vehicle are regarded as rigid components, neglecting their elastic deformation during vibration.

3. Linear springs and viscous dashpots represent the connections between car body, bogies and wheel-sets.

4. Each vehicle body has five DOFs. These are, lateral displacement, roll displacement, yaw displacement, vertical displacement, and pitch displacement. Each bogie has another five DOFs; lateral displacement, roll displacement, yaw displacement, vertical displacement and pitch displacement. And finally each wheel has three DOFs; lateral displacement, roll displacement and vertical displacement.

After these simplifications, each vehicle with 2 bogies and 4 axles has 27 DOFs. The principal difference between one research and the other is the selection of the degrees of freedom of the wheel-set that relates the interaction between rail and wheel.

The description above is related to non-articulated trains. Nevertheless, Xia [15] developed a description for articulated trains. The front and the rear locomotives have

two independent bogies with four axles and can be modeled as in the description given before. The transition vehicle has an independent bogie and the other bogie is shared with the next articulated vehicle. The carriages in the middle share both bogies. It can be seen that the DOFs change from one vehicle to another. The conclusion of the study on the behavior of the articulated train was that, the articulated train has a good running property at high speed, helping to reduce the impact on the bridge structures. In the Figure 2 the dynamic model of an articulated vehicle element is depicted.
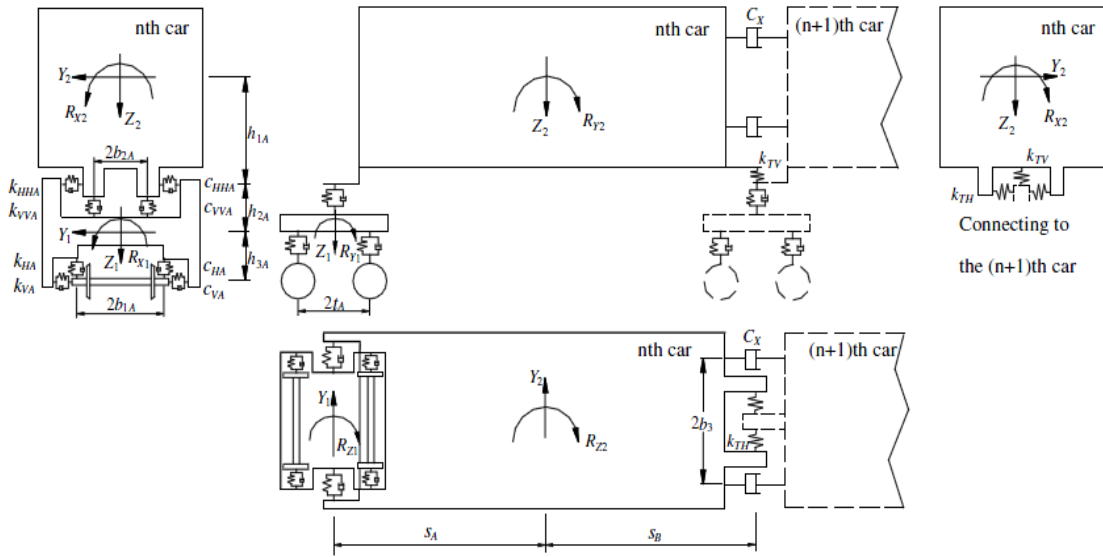
Figure 2. Dynamic model of an articulated vehicle element from [14]

Given the previous assumptions and assuming small vibrations for each part that makes up the vehicle element, the dynamic equation governing the motion of the vehicle can be defined as:

$$[M_V](\ddot{u}_V) + [C_V](\dot{u}_V) + [K_V](u_V) = (F_V) \tag{1.1}$$

where [M$_V$], [C$_V$], [K$_V$] are the matrices of mass, damping and stiffness of the vehicle respectively. ($\ddot{u}_V$), ($\dot{u}_V$), (u_V) are the vectors of displacement, velocity and acceleration respectively.

After getting the model for the vehicle, the bridge model could be made based on the following assumptions:

1. The relative displacement between the track and the bridge deck are not taken into account.

2. The vibration modes of the girder are the same as the vibration modes of the bridge deck.

3. Since the mass of the bridge is much bigger than the masses of the wheels, the wheel masses are not taken into account.

4. The cross-sectional deformation in the girder is negligible and the movement of any point of any section can be defined by the lateral displacement, vertical displacement and rotation.

When a train runs on a bridge, the forces from the wheels have to be transmitted to the bridge deck trough the track. The bridge is defined by a finite element method. Assuming small vibrations for each part of the bridge, the dynamic equation that governs the motion of the bridge system can be defined as:

$$[M_B](\ddot{u}_B)+[C_B](\dot{u}_B)+[K_B](u_B)=(F_B) \tag{1.2}$$

Where [M$_B$], [C$_B$], [K$_B$] are the matrices of mass, damping and stiffness of the bridge system respectively. $\{\ddot{u}\}$, $\{\dot{u}\}$, $\{u\}$ are the vectors of displacement, velocity and

acceleration of the bridge system respectively. $\{F_B\}$ is the vector of the forces transmitted from the wheels to the deck bridge through the track.
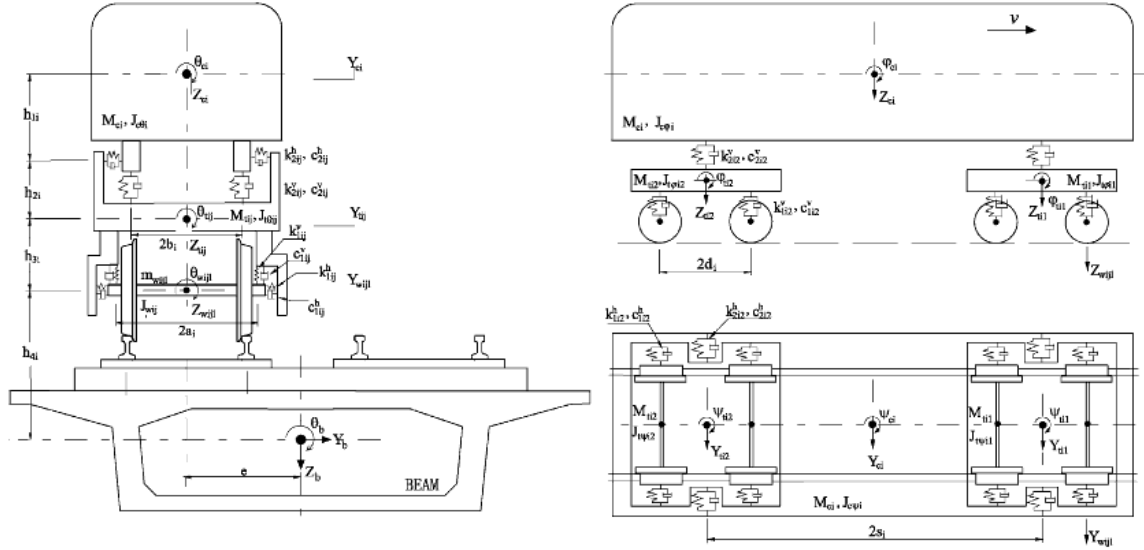
Figure 3. Dynamic interaction of vehicle and bridge from [15]

The interaction between the structure and the train (Figure 3) increases in importance as the train load and train speed is increase. When a train runs on the bridge, the bridge suffers from deflection and in turn forces the unsprung mass located on some parts of the axle of the train, to move in rhythm with the bridge motion. It is for this reason that the forces transmitted from the train to the bridge not only depend on the weight of the load but also depends on the relative displacement between other variables like inertia of the train axles or velocity of the spring of unsprung components.

The interaction between bridge and vehicle is produced in the contact between the wheel-set and the rail under the following assumptions [14]:

1. The relative displacement between the bridge deck and the track are neglected. The elastic effect of the ballast, fasteners and rail pads are also neglected.

2. The cross section deformation of the girder is considered in the modal analysis.

Assuming that the vibration amplitude is very small in each component of the vehicle and the bridge, the dynamic equation for the coupled bridge-train system using the equilibrium conditions, can be defined as [14]:

$$\begin{bmatrix} M_{vv} & 0 \\ 0 & M_{bb} \end{bmatrix} \begin{pmatrix} \ddot{u}_v \\ \ddot{u}_b \end{pmatrix} + \begin{bmatrix} C_{vv} & C_{vb} \\ C_{bv} & C_{bb} \end{bmatrix} \begin{pmatrix} \dot{u}_v \\ \dot{u}_b \end{pmatrix} + \begin{bmatrix} K_{vv} & K_{vb} \\ K_{bv} & K_{bb} \end{bmatrix} \begin{pmatrix} u_v \\ u_b \end{pmatrix} = \begin{pmatrix} F_v \\ F_b \end{pmatrix} \tag{1.3}$$

where all the variables have been defined above and the subscripts "v" represents vehicles and the subscripts "b" represents bridge.

The most common calculation method used by Xia in the majority of his researches, [15], and also used by many investigators to solve the interaction between bridge and vehicle is the Newmark-β method. This method is unequivocally convergent and the displacement, velocity and acceleration of the bridge-vehicle system are obtained within a certain time-step show in the flowchart of Figure 4.
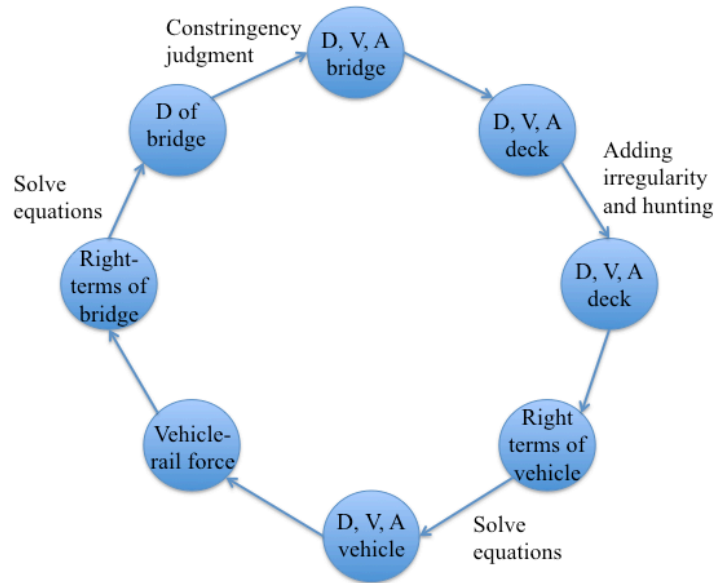
Figure 4. Flow chart of Newmark-β iteration program from [15]

Another important factor to be taken in account in the study of the interaction between vehicle and bridge is the resonance. The analysis of the resonance mechanism was also studied by Xia [16] with the conclusion that the resonant vibration of vehicle-bridge can be divided in four, depending on their generation mechanisms:

1. Bridge resonance stimulated by periodically moving load series corresponding to moving vehicles.

2. Bridge resonance stimulated by loading value corresponding to the moving loads that represent the different vehicles axels.

3. Bridge resonance stimulated by the rocking of moving vehicles induced by track irregularities and hunting movements.

4. Vehicle resonance stimulated by the vehicle regularly arranged to the different bridge spans and their deflections.

1.3. Definition of impact factor and related code values

Conventionally, the dynamic load can be considered as an equivalent static load. It is considered as the effect of a static load amplified by the impact factor. Basically, the interaction of the moving vehicle and the bridge structure causes an increase in the traffic load, which is described as impact factor. In other words, it represents the static equivalent of the dynamic vibration effects [15]. Therefore, the impact factor (IF) can be derived from the maximum value of dynamic and static responses (deflection or stress) [17]:

$$IF = \frac{D_{dyn} - D_{st}}{D_{st}} \Rightarrow \frac{D_{dyn}}{D_{st}} = 1 + IF \qquad (1.4)$$

According to the related reference, the impact factor based on deflection is larger than those based on other responses such as acceleration [18]. Therefore, in this thesis the calculation of impact factor considered dynamic and static deflection at the midpoint of bridges.

In most current design code, bridge span length (L) has been recognized as the only effective parameter affecting dynamic reaction for bridge design. For instance AASHTO manual suggests Eq.(1.5) for impact factor [19]:

$$IF = \frac{50}{L(ft) + 125} = \frac{15.24}{L(m) + 38.1} \leq 30\% \qquad (1.5)$$

For steel railway bridge, American railway bridges manual [20] proposed Eq.(1.6) to account for the vertical effect of the dynamic effect excluding the rocking effect (20% of live load) which is created by the transfer of load from the wheels on one side of a car or locomotive to the other side from periodic lateral rocking of the equipment.

$$IF = \begin{cases} 40 - \dfrac{3L^2(ft)}{1600} = 40 - \dfrac{3L^2(m)}{148.6} \Rightarrow L \le 80\,ft = 24\,m \\ 16 + \dfrac{600}{L(ft)-3} = 16 + \dfrac{182.9}{L-9.1} \Rightarrow L \ge 80\,ft = 24\,m \end{cases} \tag{1.6}$$

In AREMA Specifications [20], for train speeds below 60 mph, for all spans carrying equipment without hammer below and for all spans other than truss spans carrying equipment with hammer below, the values of the vertical effects of the impact equations shall be multiplied by the factor:

$$1 - \frac{0.8}{2500}(60 - S)^2 \ge 0.2 \tag{1.7}$$

where S= speed in mph.

Moreover, the Japanese Specification for Highway Bridges (1980) uses an impact factor formula similar in format to that of AASHTO [19] as defined in Eq.(1.5). On the other hand, the Iranian Specification for Highway Bridge [18] design uses formulas (1.9), for impact consideration:

$$IF = \frac{20}{L(m)+50} \tag{1.8}$$

$$IF = 0.3 - 0.005L(m) - 0.15 , h \ge 0 \tag{1.9}$$

Where L is the span of a straight girder and h is the depth of fill, both in meters. According to the Japanese formula, the maximum DLA could be 0.4, while the Iranian and code limits it to 0.3.

The French Cahier des Prescriptions Communes (1973) provides the following formulas, (6) and (7), for the impact factor, where again L is the span in meters [21]:

$$IF = \frac{0.64}{0.2L(m)+1} \quad \text{(For concrete bridge)} \tag{1.10}$$

$$IF = \frac{0.80}{0.2L(m)+1} \quad \text{(For steel and composite bridge)} \tag{1.11}$$

In some bridge design codes, such as the OHBD (Canada) [22] and Australian manual [23], impact factor is measured based on the first vibration frequency of the bridge. For instance, OHBD specified impact factor equal to 0.2, 0.4 and 0.25 for bridges with a first natural frequency less than 1 Hz, between 2.5 and 4.5 Hz and greater than 6 Hz, respectively. For points between 1-2.5 Hz and 4.5-6 Hz the value of impact factor varies linearly.

The impact factor relations in Figure 5 are drawn based on bridge span length according to different codes [24]. Comparison of impact factor values calculated from various codes shows that in span ranges of 25 to 50 m, the OHDB suggests higher values for (IF) than others, while for smaller spans, AREMA and Japan manuals are more conservative.
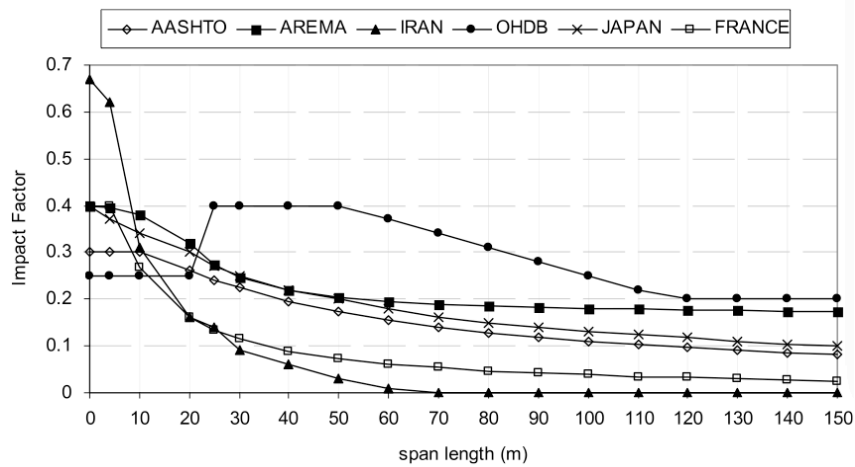
Figure 5. Impact factors based on various codes [24]

1.4. Study objective of this thesis

The main objective of this thesis is to establish a 2-D dynamic model in Matlab to study the dynamic properties of the testing bridges especially the impact factor of the specified train to the bridge. The objectives are detailed as follows:

- Test and obtain the real dynamic properties for the target steel bridge.

- Establish a 2-D model to estimate the dynamic response of the bridge and compare to the testing data.

- Analyze trainload to obtain the critical speed of particular trains to the target bridge.

- Verify the AREMA impact load

- Obtain the real impact factor to help and improve load rating.

Chapter II

Field Testing and Instrumentation

2.1. The field instrumentation

The purpose of the field testing can be summarized as following:

- Obtain structural response (strain, deflection and velocity) under dynamic rail car loading.

- Analyze the testing data to evaluate the condition of the bridge.

- Obtain the natural frequency of the bridge

- Validate and calibrate the model.

Table 1 lists the dates when the Rutgers Team (RT) went to complete field instrumentation and field testing of specified bridge. The RT spent about 8 hours to finish installing the strain transducer and attached the reflective tape on September 22nd, 2011. On September 23rd and 30th, 2011, the RT went to test the bridge.

Table 1. Sensor Installation and testing dates for target bridge

Testing on NJ Transit Railroad Bridges	
Raritan Valley Line MP 31.15 (Installation)	09/22/2011(Thursday)
Raritan Valley Line MP 31.15 (Testing)	09/23/2011(Friday)
Raritan Valley Line MP 31.15 (Testing)	09/30/2011(Friday)

2.2. Testing equipment

2.2.1. Structural Testing System

The Structural Testing System (STS), a modular data acquisition system, is designed and made by Bridge Diagnostics, Inc. (BDI) of Boulder, Colorado. The system consists of three parts, strain transducers, one main processing unit that samples data, and six junction nodes that is connected with strain transducers by cable and transfer data to main unit via wireless signal. The strain transducers can be mounted to different kinds of structural elements with C-clamps or bolts. Each transducer was assigned with a unique identification number and microchip so that the transducer can be identified easily either for the system or users during testing. Figure 6 shows a strain gages installed on the girder of a railway bridge. The system needs transducer calibration factors that are stored in the configuration files and are applied automatically. Figure 7 and Figure 8 show the main unit and technical specifications of the Wi-Fi system, respectively. After the test has

been completed, user can download the data from the STS unit to a laptop computer. The STS data files, which contain test information such as date, time, duration, strain transducer ID numbers, and the stress data is in ASCII text format.
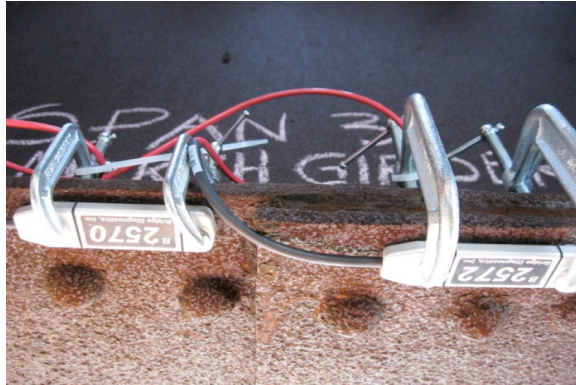
Figure 6. STS Strain Transducer Installed on the bottom flange of a Bridge Superstructure Member

Figure 7. Wireless Data Collection System, Bridge Diagnostics Inc.

Technical Specifications

Channels	4 to 64, Expandable in multiples of 4
Hardware Accuracy	± 0.2% (2% for Strain Transducers)
Sample Rates	Max 500 Hz (Internal over-sampling rate is 19.5-312 KHz)
Max Test Lengths	21 minutes at 100 Hz. 128K samples per channel maximum test length
Gain Levels	1, 2, 4, 6, 16, 32, 64, 128
Digital Filter	Fixed by selected sample rate
Analog Filter	200 Hz, -3db, 3rd order Bessel
Max. Input Voltage	10.5 VDC
Power	9.6V NiMH rechargeable battery (Programmable low-power sleep mode)
Alternative Power	9-48 VDC input
Excitation Voltages Standard: LVDT/Other	5 Volts DC 5.5 Volts DC
A/D Resolution	0.3uV bit (24-Bit ADC)
PC Requirements	Windows 2000 or higher
PC Interface	Wi-Fi Ethernet 802.11b: 10/100 Mbps
Auto Zeroing	Sensor automatically zero before each test
Enclosures	Aluminum splash resistant
Sensor Connections	All aluminum military grade, circular bayonet "snap" lock
Vehicle Tracking	BDI AutoClicker, switch closure detection
Sensors	BDI Intelliducer Strain Transducers Also supports LVDTs, foil strain gages, accelerometers, various DC output sensors Single RS232 serially-interfaced sensor
On-board PC Processor: RAM	520 MHz Intel XScale PXA270 64MB
Dimensions Base Station: STS 4 Channel Unit:	10" x 6" x 4" 11" x 3.5" x 3.25"

Figure 8. Technical Specifications of Wi-Fi Data Collection System

(Source: http://www.bridgetest.com/products/STS3-WiFi.pdf)

2.2.2. Laser Doppler Vibrometer

The Laser Doppler Vibrometer (LDV) (Figure 9), a non-contact measuring device, was adopted to measure displacement and velocity of a remote point. Once the distance between the laser head and the reflective target changes, a Doppler shift in the light frequency will be decoded into displacement and velocity. The system is composed of three parts, the helium neon Class II laser head, the decoder unit and the reflective target,

which is attached to the structure. The laser head need to be adjusted to a tripod that is positioned right underneath the target to get best signal. This needs to be finished prior to a test. The signal strength is read on a scale on the laser head. The reflective target such as retro-reflective tape can provide good signal.
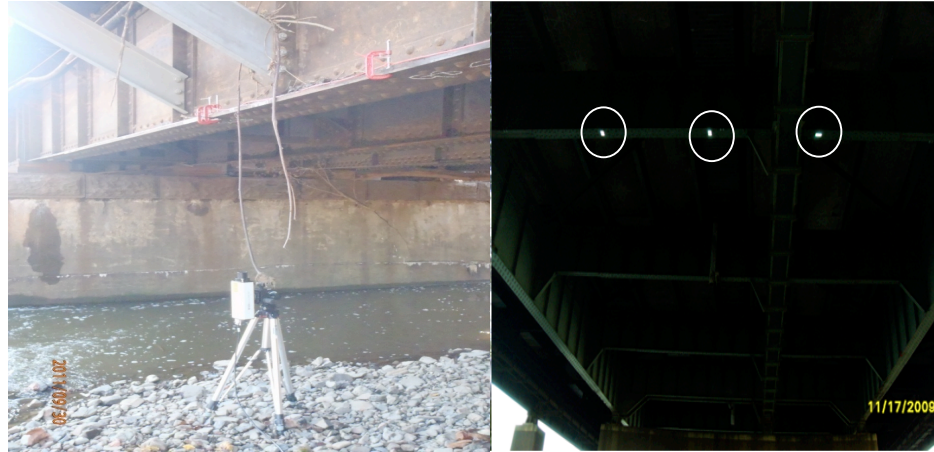
(a)   (b)

Figure 9. (a) Laser Doppler Vibrometer and (b) locations of reflective targets for Measuring Deflections

2.3. Testing plan

The following is a brief description of the selected bridge (Raritan Valley Line 31.15) from the Inspection Report four [25]:

1. Name: Raritan Valley over Middle Brook

2. Structural type: Steel through girder, open hearth steel

3. 8 Girders (2 active tracks)

4. 4 Simply supported spans

5. Span length: 40 feet (12.2m)

The bridge is a four span, open deck, riveted deck plate girder bridge. It is supported by one stone masonry abutment, one concrete abutment and 3 concrete piers. This structure carries two active tracks on a tangent horizontal alignment which are supported by G5 through G8. The tracks have been removed from the top of G1 through G4. The overall condition of the structure is poor from [25]. A general view of the bridge and the instrumented span are shown in Figure 10. Figure 11 and Figure 12 shows the location of the bridge from the google map.

The strain transducers that were installed at this structure were mainly focused on the girder G8 in span 2 below the active track. For the girders G5-G7 in span 2 and girders G5-G8 in span 3, there were also some transducers installed to have a thorough understanding of the structural response of the structure as well as the train speed.

Figure 10. General View of the Bridge from Cycle Report 4 (North elevation, looking south)

Figure 11. Location of bridge from Google map

Figure 12. General view from the Google map

On November 22, 2011, the RT went to the Raritan Valley Line MP 31.15 bridge site to install strain transducers and reflective tape for the LDV. The installation took around 8 hours. After installation of the equipment, the RT tested the running train to collected strain, displacement and velocity of the beam. Figure 13 shows the testing systems set up for span 2. The junction nodes that connect to the stain transducers via cable were put on the pier of span 2. Testing data was transferred from the nodes to the main unit by a wireless signal. Then the computer can retrieve the data by the wireless signal from the main unit. Wireless structural testing system is a convenient way to conduct field testing on a structure where it is not practical to setup the cable-based testing system. Figure 14 shows the locations of the strain gages that were installed on Span 3 of Raritan valley Line MP 31.15 bridge structure.
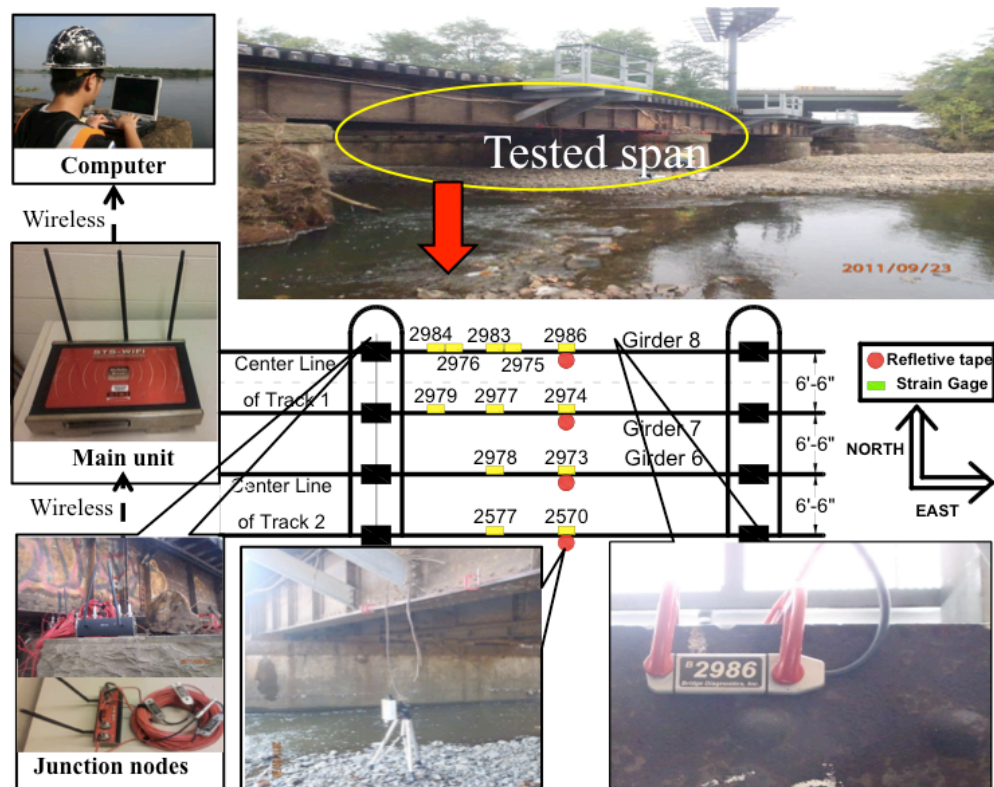
Figure 13. Wireless structural testing systems in span 2
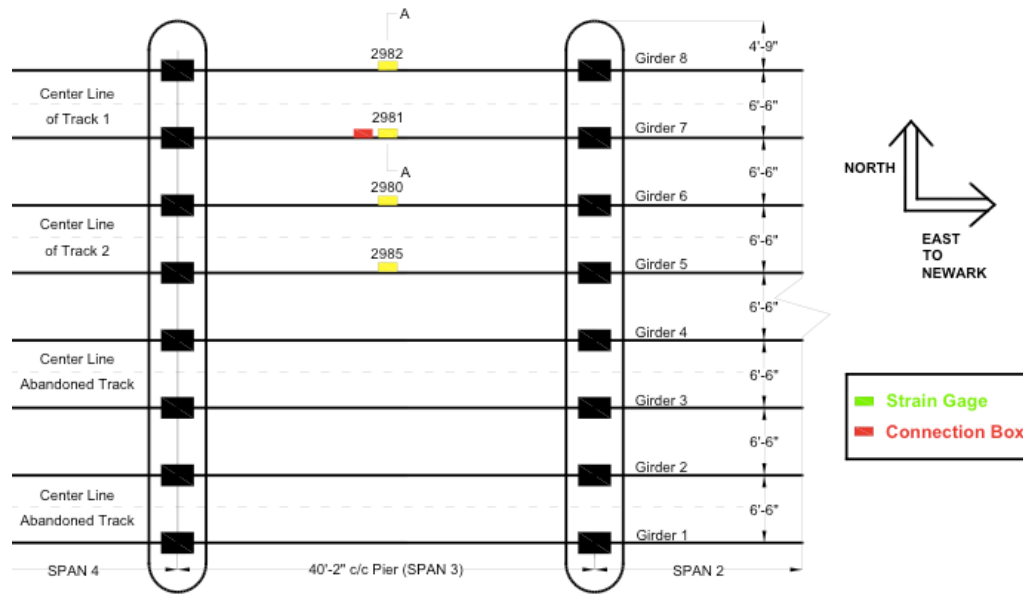
Figure 14. Location of strain gages in span 3

The following are a description of the exact location of each strain transducer:

- Section A-A is the mid span section (Girders G7 and G8)

- Section C-C is the second cut off point (about 8'-8.5'' from the support end of the girder). Section B-B is the first cut off point (about 5'from the support end of the girder).

- Strain transducer numbered 2984 and 2979 are installed on the first bottom cover plate of the first cut-off point.

- For span 3, strain transducers were installed at the mid span of each girder under the active track (G5 through G8).

Figure 15 shows the space below the desired span 2 and Figure 16 gives a bottom view (looking upwards) of span 2 as well as the corresponding location of the strain transducers.

Figure 15. Space under the span 2

Figure 16. Bottom view of the span 2 (G5-G8, only show strain transducers on G7 and

G8)

Figure 17 through Figure 19 give more details on the exact locations of strain transducers installed on this structure as well as the cross sections of the typical beams as built. Section B-B and Section C-C are similar to the mid span cross section (Section A-A)

except for the thickness of flange and cover plate. Table 2 shows a summary of the thickness of girders' flange in span 2.

Table 2. Flange thickness of girders in span 2.

Section	Thickness of top flange + cover plate	Thickness of bottom flange + cover plate
A-A	1.4375''	1.4375''
B-B	1	0.5
C-C	1	1
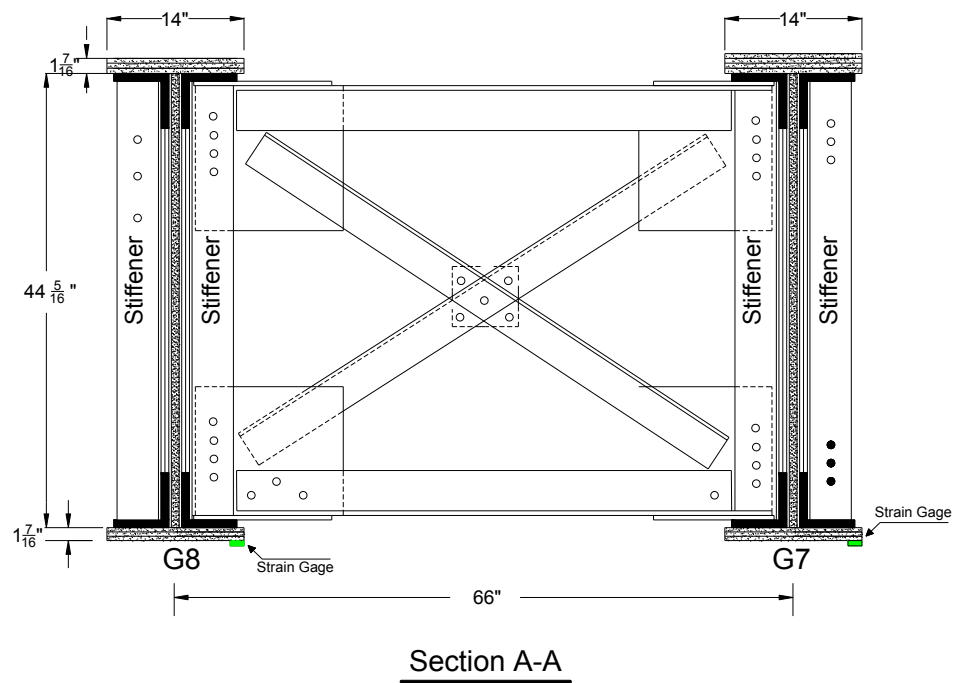
Figure 17. Girder cross section of mid-span point in span 2
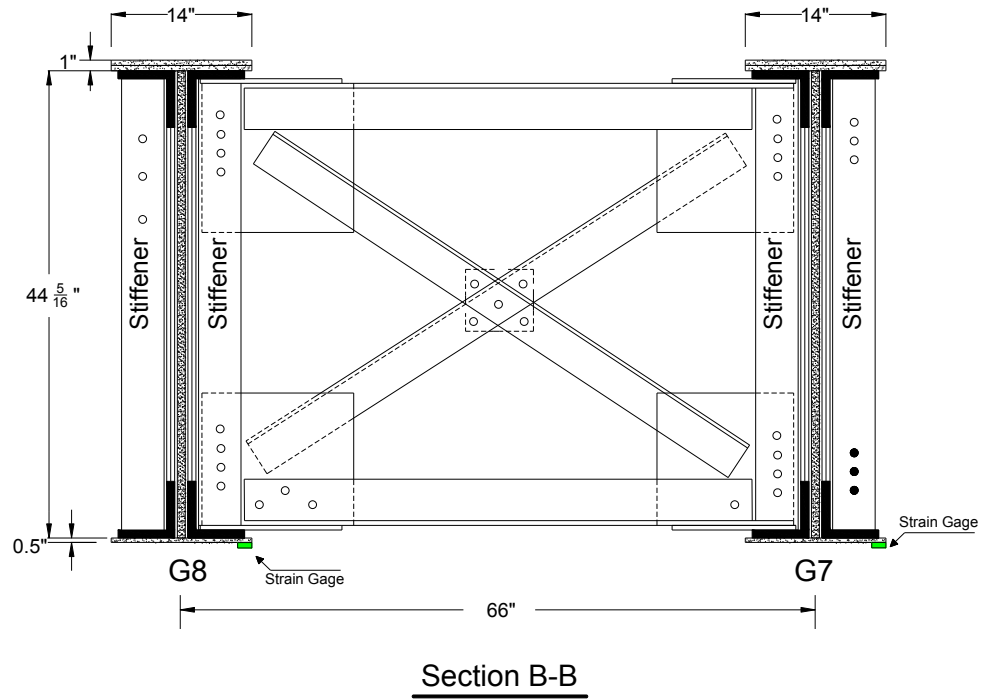
Figure 18. Girder cross section at first cut-off point in span 2
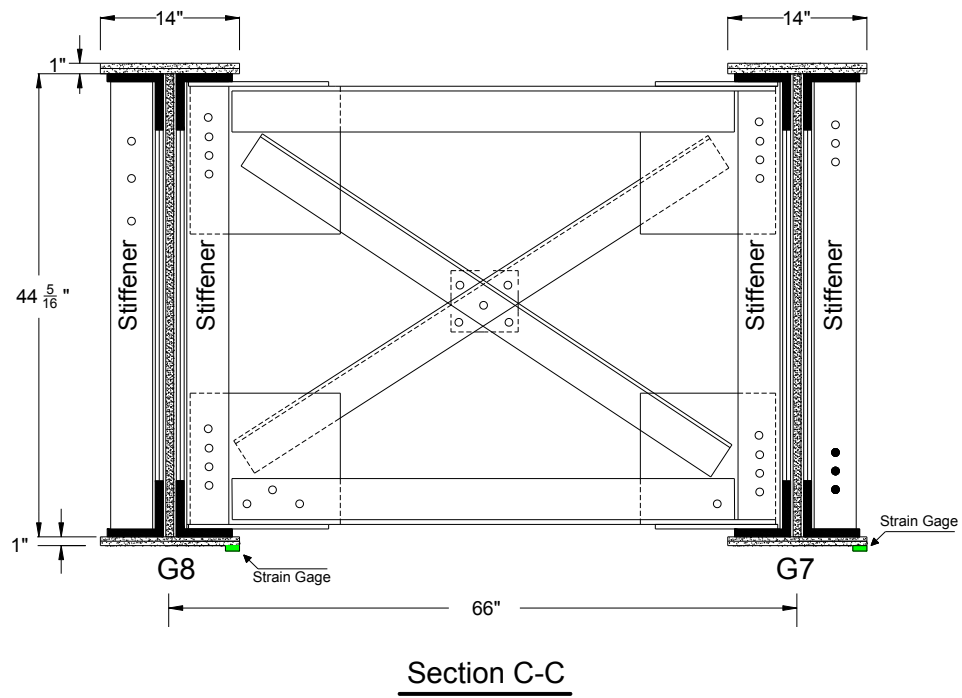
Figure 19. Girder Cross section at second cut-off point in span 2

Figure 20 through Figure 23 show more photos taken during the installation and testing. Figure 23 is the photo of the tested trains. On the Raritan Valley Line, the in-service NJ Transit passenger train consists of one PL-42 locomotive car followed by six passenger cars. The detailed configuration of each car will be given later.

Figure 20. Strain transducers Installation

Figure 21. Span 2 (desired span)

Figure 22. Junction nodes positioned on pier

Figure 23. Tested train driving through the bridge

After collecting the field-testing data, NJ Transit provided the RT with the tested train information according to the specified arrival time of each run. With the train information, the RT could validate the dynamic model with the specific train model.

The tested train information on September 30th is listed in Table 3. The trains running on Track 1 is westbound going from Bound Brook to Bridge Water while that running on Track 2 is eastbound going from Bridge Water to Bound Brook.

According to NJ Transit, the locomotive running on the Raritan Valley Line is Locomotive car PL-42 whose total weight is 286K. Figure 25 through Figure 27 show the configuration of a PL-42 locomotive, passenger train, ALP-46a and AREMA conference 286 Railcar, respectively. PL-42 locomotive and the passenger train are the railcars running on the Raritan Valley Line while ALP-46a locomotive car is the locomotive running on the North Jersey Coast Line Bridge which will be discussed in the results. The AREMA conference 286K railcar is the tested train on the Bergen County Line, which will also be introduced in the result part.
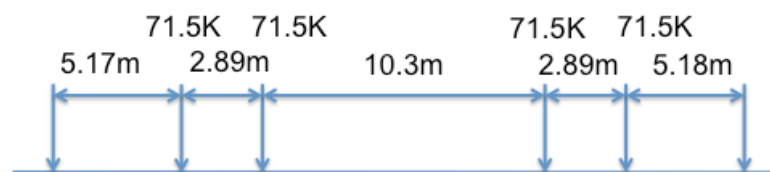
Figure 24. Configuration of PL-42 locomotive car from NJ Transit
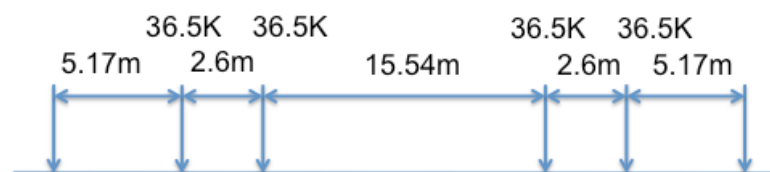
Figure 25. Configuration of passenger train in Raritan Valley Line
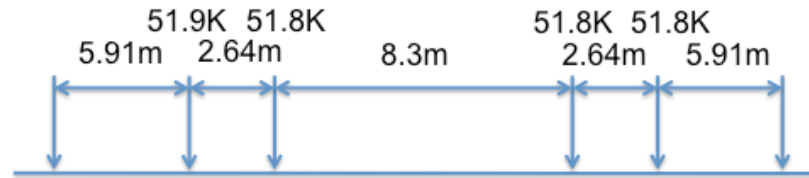
Figure 26. Configuration of ALP-46a locomotive car from NJ Transit
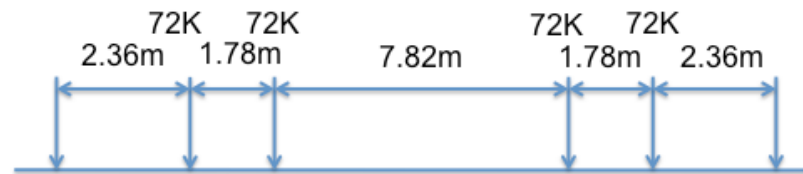
Figure 27. Configuration of AREMA conference 286K railcar

Table 3. Train information for Raritan Valley line on 09/30/2011

Run #	Arrival time	Direction	Track	Train #	laser
7	8:44 AM	Bound brook-Bridge water (W)	1	5413	N/A
8	8:52 AM	Bridge water-Bound Brook (E)	2	5426	N/A
9	9:49 AM	Bound brook-Bridge water (W)	1	5415	G8
10	9:56 AM	Bridge water-Bound Brook (E)	2	5730	G8
11	10:51 AM	Bound brook-Bridge water (W)	1	5719	G8
12	10:56 AM	Bridge water-Bound Brook (E)	2	5432	G6
13	11:49 AM	Bound brook-Bridge water (W)	1	5421	G8
14	11:56 AM	Bridge water-Bound Brook (E)	2	5434	G6
15	12:49 PM	Bound brook-Bridge water (W)	1	5423	G7
16	12:55 PM	Bridge water-Bound Brook (E)	2	5736	G5
17	1:48 PM	Bound brook-Bridge water (W)	1	5725	G7
18	1:56 PM	Bridge water-Bound Brook (E)	2	5438	G5
19	2:51 PM	Bound brook-Bridge water (W)	1	5427	G8
20	2:56 PM	Bridge water-Bound Brook (E)	2	5440	G5

Figure 28 through Figure 32 show the strain data collected at the mid-span and cut-off points of each girder. The strain data collected in the mid-span of girders are 135 με from G8 in span 2, 105 με from G7 in span 2, 105 με from G6 in span 2, 90 με from G5 in span 2, 115 με from G8 in span 3, 120 με from G7 in span 3, 105 με from G6 in span 3 and 120 με from G5 in span 3. Strain data B2986 in Figure 29 shows that the maximum strain data collected was from girder 8 in span 2 while strain data B2570 in Figure 32 shows the minimum strain data is 90 με from G5 in span 2. This suggests that G5 in span 2 is stronger than the other girders both in span 2 and span 3 and G8 in span 2 is the weakest girder. From the analysis above, the field measurement agrees well with the cycle report that was based on the physical inspection of the bridge. Taking the Young's modulus is 29000 ksi into account, the maximum stress in the girders is 4 ksi. According to the field testing results, the steel plate girders are in good condition considering that this bridge has been in service for more than 100 years. Also the strain data will be compared with the analytical results from the dynamic model and discussed in the result part.
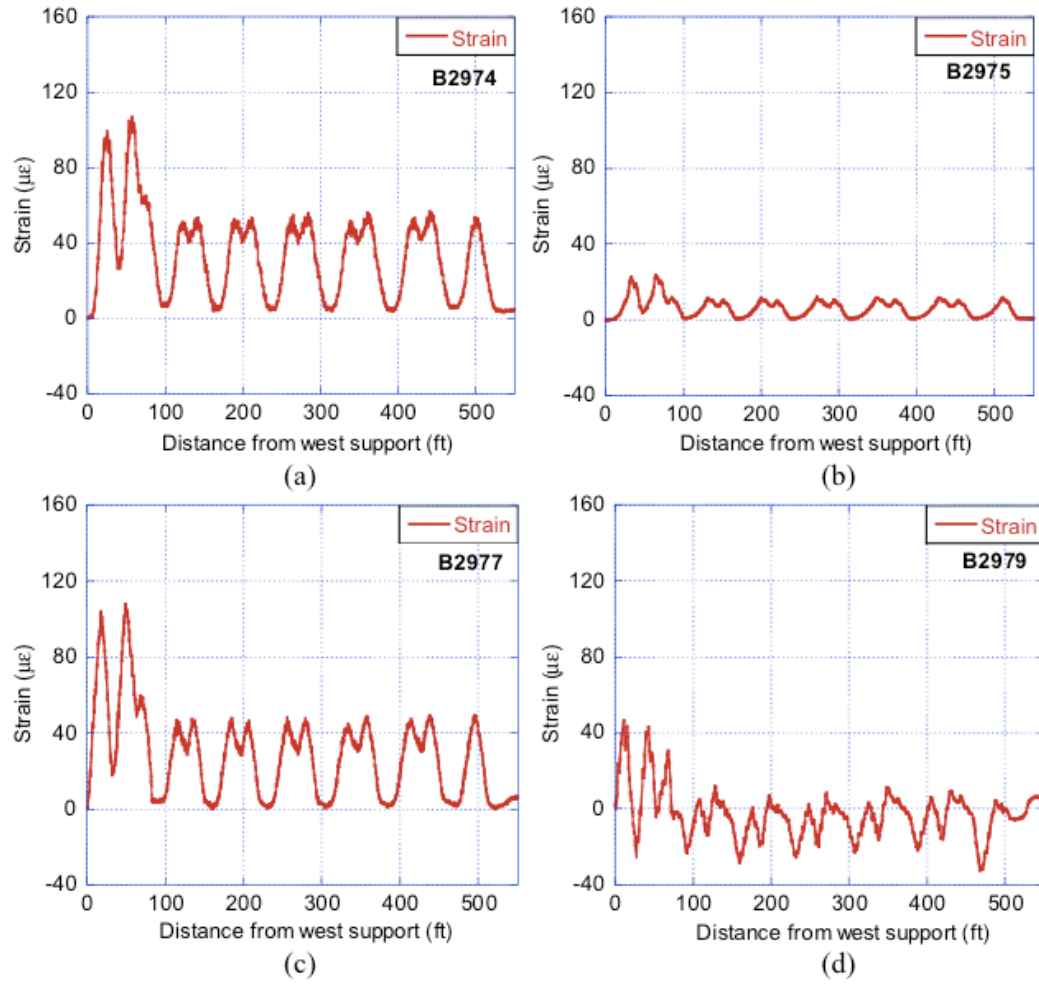
Figure 28. Strain data measured from Test Run #9 at Strain Transducer No.: (a) B2974,

(b) B2975, (c) B2977, (d) B2979
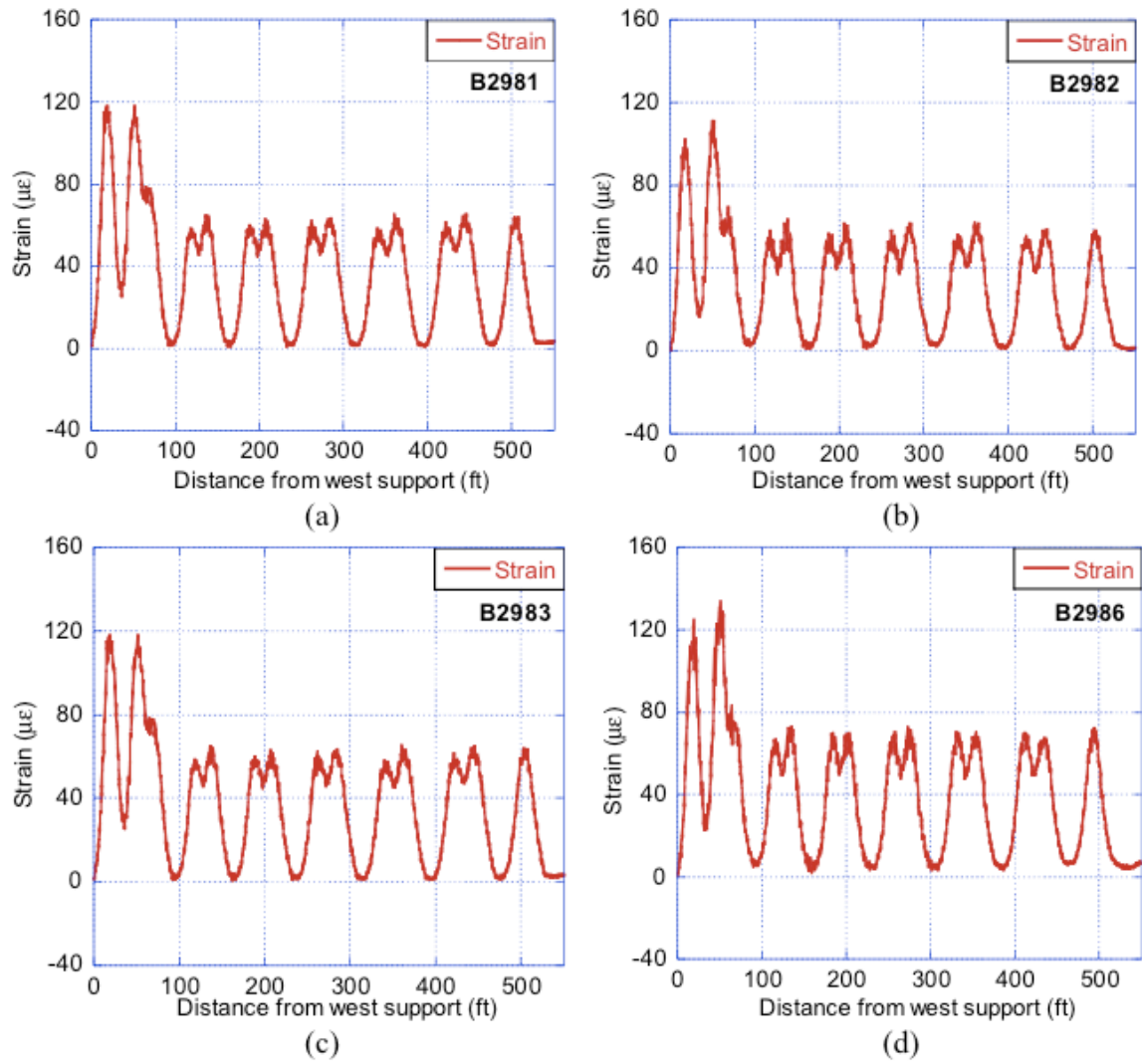
Figure 29. Strain data measured during Test Run #9 at Strain Transducer No.: (a) B2981, (b) 2982, (c) B2983, (d) B2986
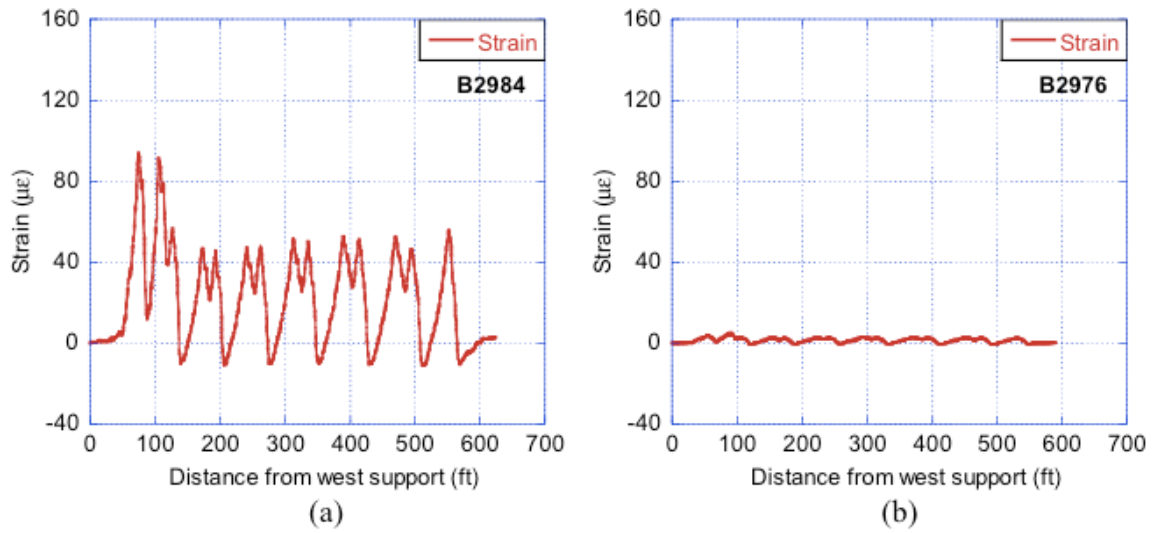
Figure 30. Strain data measured during Test Run #9 at Strain Transducer No.: (a) B2984,

(b) 2976
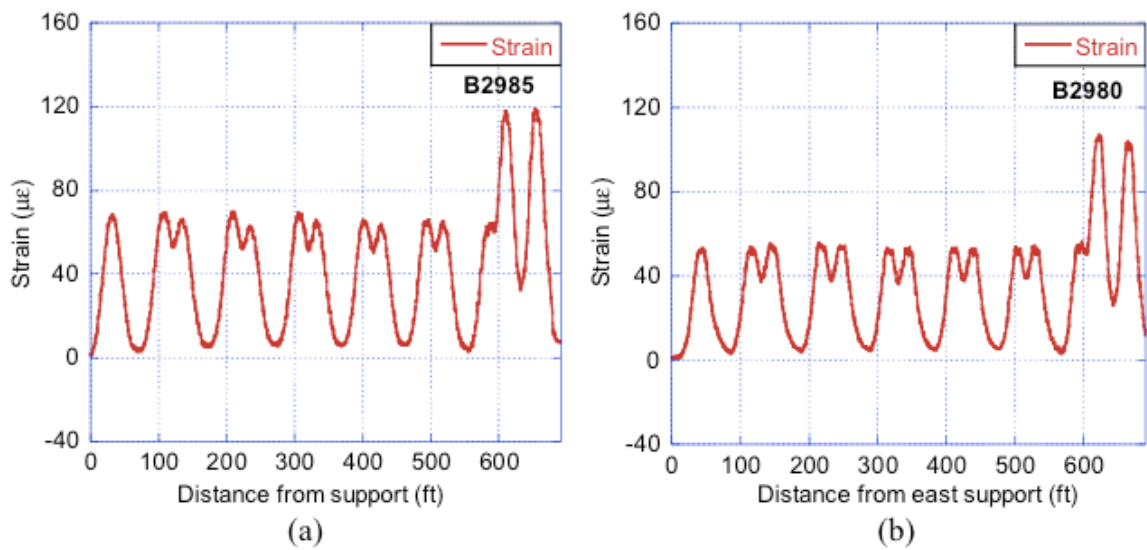
Figure 31. Strain data measured during Test Run #10 at Strain Transducer No.: (a)

B2985, (b) B2980
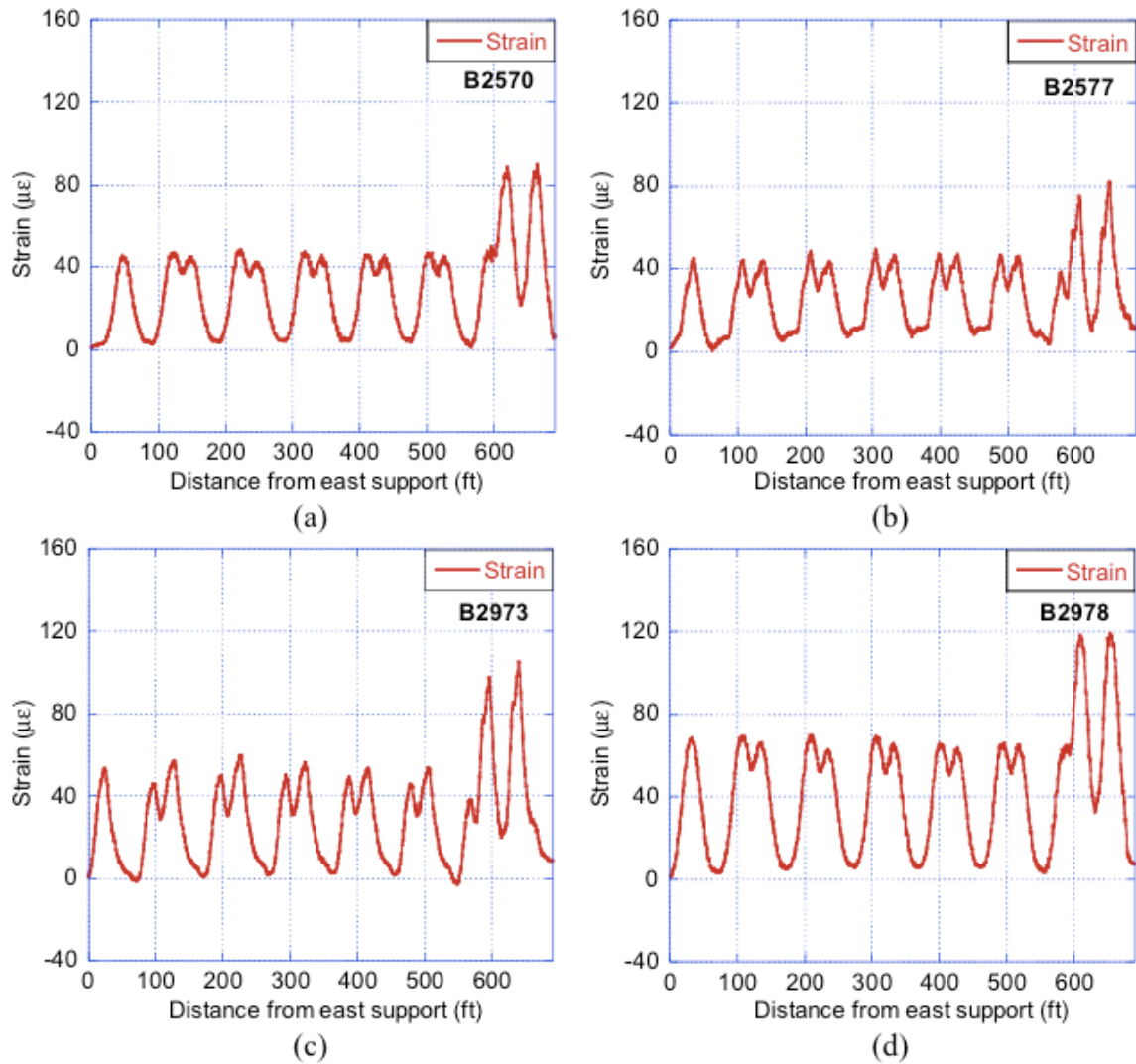
Figure 32. Strain data measured during Test Run #10 at Strain Transducer No.: (a)

B2570, (b) 2577, (c) B2973, (d) 2978

Figure 33 shows typical deflection and velocity data obtained from run 9 and run 12. From the tested results below, the maximum deflection at the midspan is 4.2 mm for both girder 8 and girder 6. The velocity result can be used to conduct a Faster Fourier Translation (FFT) to obtain the real natural frequency of the bridge. This will also help to improve the accuracy of the dynamic model.
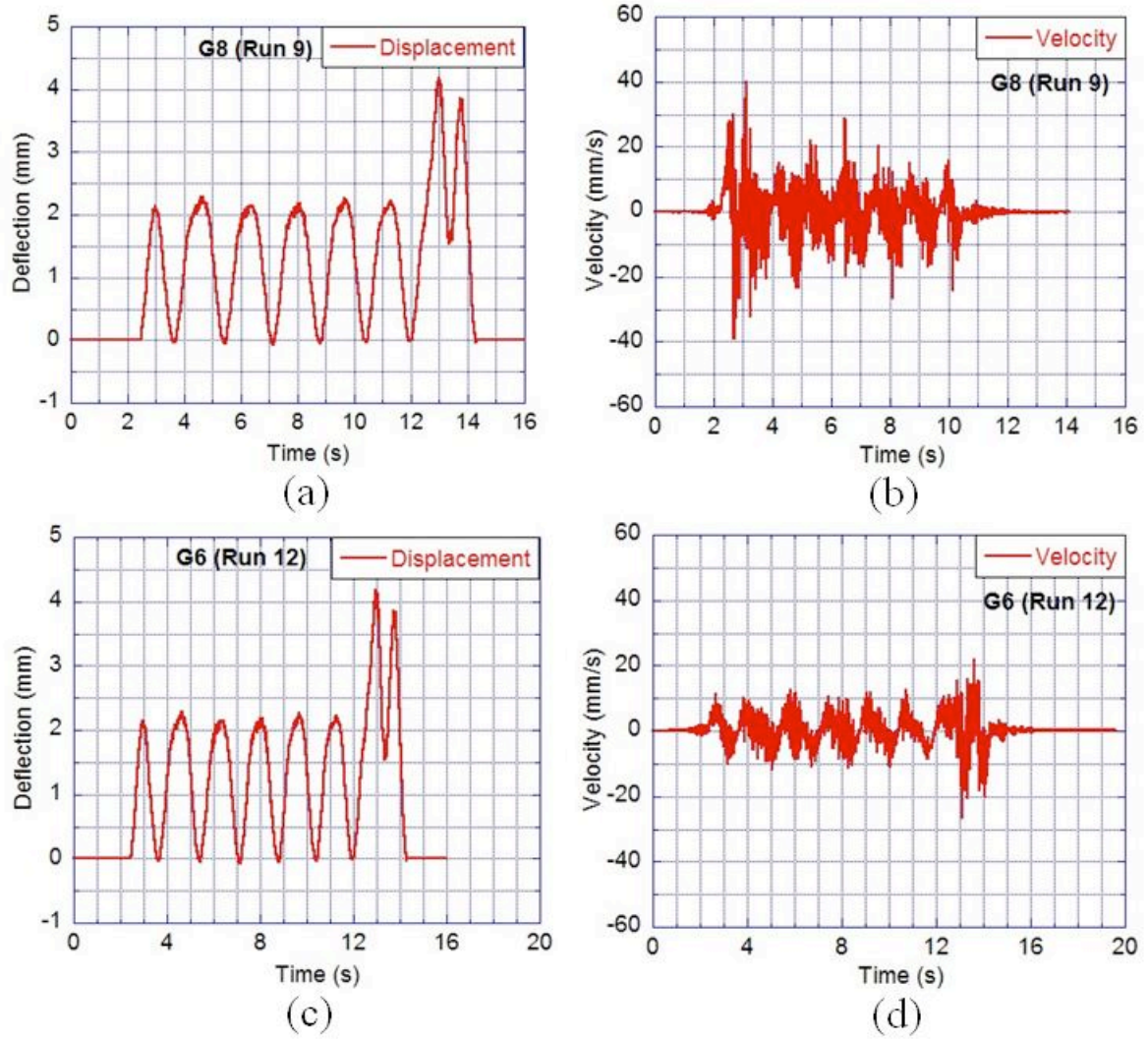
Figure 33. Typical deflection and velocity at the mid-span of the testing girder: (a) Run 9 displacement; (b) Run 9 velocity; (c) Run 12 displacement; (d) Run 12 velocity

Chapter III

Dynamic Model of the Bridge

3.1. Important theoretical concepts

In this section, important concepts will be introduced to explain the theoretical background of bridge-vehicle interaction.

In the analysis of the dynamic response of the beam, there are two important beam theories including Euler-Bernoulli beam theory (shear-indeformable model) and Timoshenko beam theory (shear-deformable model). Since the Timoshenko beam theory is of a higher order than the Euler-Bernoulli theory, it is known to be superior in predicting the transient response of the beam. The superiority of the Timoshenko model is more pronounced for beams with a low aspect ratio. But the Euler-Bernoulli beam theory gives good results for slender, long beam. In this thesis, Euler-Bernoulli beam theory will be introduced and applied in the dynamic model.

In order to carry out the structural dynamic analysis, two methods are used in most of the cases; the mode superposition method and the direct integration. The direct integration method does not require any transformation of the equation, and uses a numerical step-by-step procedure. For this reason, this method is considered as direct. For systems with linearity and without coupled damping, mode-superposition methods were employed to

obtain the dynamic response of linear multi-degree of freedom by transforming the equation of motion to principal coordinates and solving the resulting set of uncoupled equations of motion. In this part, the mode-superposition method will be explained and applied in the dynamic model. Furthermore, the damping models and mass matrix will be explained.

3.1.1. Euler-Bernoulli beam theory

A beam is a structure element, which is much larger in one dimension than the other two. The axis along the principal direction can be used to define the beam. The cross section of beam is perpendicular to this axis. An assembly or grid of beams makes up the majority of the structures in civil engineering. Although currently more and more advanced tools exist for design, for example the finite element method, the beam models continue to be used in the design step, and also to validate the results obtained by computer programs.

Some beam theories have been developed through history with different assumptions and different levels of accuracy. Euler and Bernoulli developed one of the most important beam theories, namely, the Euler-Bernoulli beam theory. In the following, this theory will be briefly explained.

The cross-section is assumed as an infinitely rigid in its own plane, which means, no deformations will exist in the plane of cross-section as is illustrated in Figure 34. This is the most important assumption in this theory. Thence, the displacement field in plane can

be defined with one rotation and two translations of the rigid body. The other two assumptions related to the out-of-plane displacement field of the section are concluded as: the cross-section of a beam remains in plane and the cross-section is normal to the deformed axis of the beam during and after the deformation.
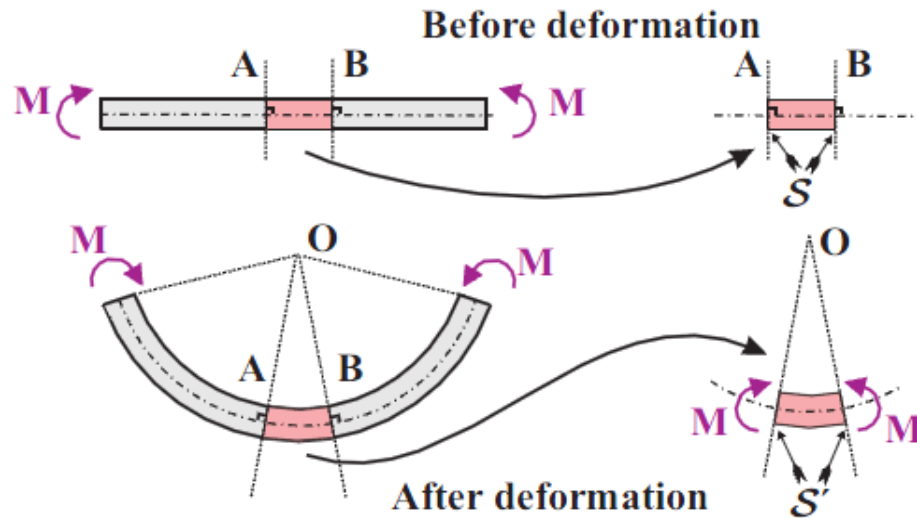
Figure 34. Long beam deformation under end bending moments from [3]

These assumptions are established under the circumstances of slender long beams made of isotropic materials and with solid cross-sections. The accuracy of the results cannot be assured if one or more of these assumptions are not fulfilled.

Fryba [8] explored the dynamic response of a simple supported beam under different kinds of moving loads by supplementing Euler-Bernoulli's differential equation based on the following assumptions: theory of small deformations, Navier's hypothesis, Hooke's law, and Saint Venant's principle.

3.1.2. Damping models

Damping is mostly used to define the physical dissipation of energy. The general mechanisms include material damping, fluid structure interaction, and friction. The materials damping is related to viscoelasticiy or other non-linear case. Linear viscoelasticity is expressed by complex modules, which are not time domain equivalent or internal states, consequently it is very difficult to incorporation it to finite element model. Also friction is quite difficult to model since it usually appears in joints.

Due to these restrictions it is a complicated process to introduce damping models to dynamic systems. There are two types of general viscous damping model: Rayleigh and modal damping. Modal damping ratio is generally used in the frequency domain while Rayleigh damping is usually used in the time domain. In this thesis, viscous damping is defined as a force that is proportional to velocity expressed as following:

$$M\{\ddot{q}(t)\} + C\{\dot{q}(t)\} + K\{q(t)\} = \{F(t)\} \qquad (3.1)$$

where M is the mass matrix, K is the stiffness matrix and C is the damping matrix which is generally a symmetric semi-positive definite matrix in order to ensure a passive system. *F(t)* is the force vector which is a function of time.

However, the viscous damping is not the best choice in order to represent the material damping. Hysteretic models better represent the material damping because in these models the dissipation force is proportional to displacement, or friction, where the

damping only depends on the direction of the velocity. Viscous damping is usually seemed to be an approximation in time domain simulation. However it is commonly used because it is a linear dissipation mechanism and gives a relevant time save in computation especially in big models.

3.1.3. Mode superposition method

The mode superposition method is commonly used to reduce the number of system's multi degree of freedom. On the other way, it is also possible to select the modes used in the response and combine them to produce the total response of the structure elements. This selection reduces the usage of computer capacity and then enabling more simulations to be performed. Due to the characteristics of the method it is impossible to integrate any non-linear behavior or un-coupled damping into dynamic model. The integration of the equation of motion can be found in [26].

As explained by previous research, Bath [26] conclude two important properties from the modes of vibration; 1) The first property states that the vibration modes of a dynamic system are orthogonal to each other with respect of the stiffness K and mass M matrices. 2) The second property indicates that the modes of vibration of a dynamic system compose a basis for the n-dimensional space.

According to the second property, we could assume the displacement matrix to be:

$$u(x,t) = \Phi(x)q(t) \qquad (3.2)$$

Where $u(x,t)$ is the displacement matrix, $\Phi(x)$ is the matrix about the modal function,

$q(t)$ is the matrix with respect to the modal coordinates.

These two properties from the modes of vibration can used to uncouple the dynamic equations of motion, which means we could transfer the coupled differential equations into n independent differential equations. It is an efficient method of solving the dynamic equations of motion.

Natural frequency and vibration modal function

Consider the partial differential equation of free motion of the beam as in Eq.(3.3)

$$m(x)\frac{\partial^2 u}{\partial t^2} + \frac{\partial^2}{\partial x^2}\left[EI(x)\frac{\partial^2 u(x,t)}{\partial x^2}\right] = 0 \tag{3.3}$$

We need to consider two types of beam before we solve to obtain the natural frequency; one is the beam with uniform section property and the other is the beam with varying section property. In the uniform beam case, the natural frequency and modal function can be easily induced by the method of separation of variables. But in the varying beam case, the solution is much more complicated.

i. Uniform beam

Eq.(3.3) becomes to (3.4).

$$m\ddot{u} + EIu'''' = 0 \tag{3.4}$$

Since this is a partial differential equation, we will try to use the method of separation of variables. Assume $u(x,t) = \Phi(x)q(t)$, where $\Phi(x)$ is the modal function, which is not changed with time t, and $q(t)$ is the modal coordinate. Substitute $u(x,t)$ into Eq.(3.4), and we get:

$$\frac{\phi''''}{\phi} = -\frac{m}{EI}\frac{\ddot{q}(t)}{q(t)} \tag{3.5}$$

In the above equation, the left part is a function of x, the right part is a function of time t. If the equation applies to all x and t, it should be equal to a constant. Then we have:

$$\frac{\phi''''}{\phi} = -\frac{m}{EI}\frac{\ddot{q}(t)}{q(t)} = a^4 \tag{3.6}$$

From Eq.(3.6), we have two independent ordinary differential equations:

$$\ddot{q}(t) + \omega^2 q(t) = 0 \tag{3.7}$$

$$\phi''''(x) - a^4\phi(x) = 0 \tag{3.8}$$

Where $\omega^2 = \dfrac{a^4 EI}{m}$ or $a^4 = \dfrac{\omega^2 m}{EI}$.

Eq.(3.7) is a single degree undamped free vibration equation with the solution as:

$$q(t) = A_1\sin\omega t + B_1\cos\omega t \tag{3.9}$$

Where A_1 and B_1 is based on the initial condition $q(0)$ and $\dot{q}(0)$. Then we have:

$$q(t) = \frac{\dot{q}(0)}{\omega}\sin\omega t + q(0)\cos\omega t \qquad (3.10)$$

Meanwhile, Eq.(3.8) is a fourth-order differential equation with the solution as:

$$\phi(x) = A\sin ax + B\cos ax + C\sinh ax + D\cosh ax \qquad (3.11)$$

Constants A, B, C and D determine the vibration shape and amplitude of the beam. They can be calculated using the boundary conditions of the beam. For the situation of a simple supported beam, the solution of the modal function is simple as shown in Eq.(3.12):

$$\phi(x) = A\sin\frac{n\pi x}{L} \qquad (3.12)$$

ii. Beam with varying cross sections

In this case, this partial differential equation cannot be transformed to an ordinary differential equation using the method of separation of variables.

Orthogonality property of the natural modes of vibration

According to the reciprocal theorem, the work that is done by the initial force of *nth* mode in *mth* modal displacement equals the work done by the initial force of *mth* in *nth* modal displacement. The theorem can be illustrated by the following equation:

$$\int_0^L u_m(x)f_{I,n}(x,t)dx = \int_0^L u_n(x)f_{I,m}(x,t)dx \tag{3.13}$$

The displacement of each point in a certain mode can be expressed as:

$$u_n(x,t) = \phi_n(x)q_n \sin\omega_n t \tag{3.14}$$

$$u_m(x,t) = \phi_m(x)q_m \sin\omega_m t \tag{3.15}$$

Corresponding initial forces of certain modes can be written as:

$$f_{I,n}(x,t) = -m(x)\frac{\partial^2 u_n^2(x,t)}{\partial t^2} = m(x)\omega_n^2\phi(x)q_n \sin\omega_n t \tag{3.16}$$

$$f_{I,m}(x,t) = -m(x)\frac{\partial^2 u_m^2(x,t)}{\partial t^2} = m(x)\omega_m^2\phi(x)q_m \sin\omega_m t \tag{3.17}$$

Substitute the above four equations into Eq.(3.13), we have:

$$\int_0^L \phi_m(x)q_m m(x)\omega_n^2\phi_n(x)q_n\, dx = \int_0^L \phi_n(x)q_n m(x)\omega_m^2\phi_m(x)q_m\, dx \tag{3.18}$$

$$(\omega_n^2 - \omega_m^2)\int_0^L \phi_n(x)m(x)\phi_m(x)dx = 0 \tag{3.19}$$

From bridge structure, $\omega_n^2 \neq \omega_m^2$, Therefore, we have the orthogonality property of simple supported beam about its mass distribution:

$$\int_0^L \phi_n(x)m(x)\phi_m(x)\,dx = 0 \qquad (3.20)$$

We can also get the second orthogonality property of the simple supported beam with respected to the stiffness:

$$\int_0^L \phi_m(x)\frac{d^2}{dx^2}\left[EI(x)\frac{d^2\phi_n}{dx^2}\right]dx = 0 \qquad (3.21)$$

3.1.4. Integration of second-order multi-degree systems

In this section, we introduced three related methods for integration of second-order systems: the Central Difference Method, the Newmark-β Method, and the Wilson-θ Method. These methods are not entirely independent. The first two methods are presented in a form appropriate for the direct integration of linear second-order systems, such as those whose damping matrix cannot be diagonalized by the system normal modes. The last technique is presented in a form that is appropriate for some classes of nonlinear second-order systems.

Central Difference Method **[27]**

The most fundamental algorithm for the approximate numerical solution of second-order ordinary differential equations arising in applications in structural dynamics is the *Central Difference Method*. The origin of its standing among all the possible finite difference equations that can be applied to the governing equations of structural dynamics is easily understood. Recall the form of the second-order ordinary differential equations of structural dynamics Eq.(3.1):

$$[M]\{\ddot{U}\}+[C]\{\dot{U}\}+[K]\{U\}=\{F\}$$

We employ the convention that $u(t_n)$ equal to u_n. The foundation of the Central Difference Algorithm is the simple finite-difference expression:

$$\dot{u}_n = \frac{u_{n+1}-u_{n-1}}{2h} \tag{3.22}$$

$$\ddot{u}_n = \frac{u_{n+1}-2u_n+u_{n-1}}{h^2} \tag{3.23}$$

The derivative at time t_n is approximated by the slope of the line passing through the values of the function at t_{n-1} and t_{n+1}. To maintain consistency in the order of approximation, the value of the second derivative is calculated as the difference of first-order forward and backward finite differences.

When the finite-difference expressions for the first and second derivative are substituted into the governing equation of motion evaluated at t_n, the discrete governing equation results:

$$(\frac{1}{h^2}M + \frac{1}{2h}C)u_{n+1} + (K - \frac{2}{h^2}M)u_n + (\frac{1}{h^2}M - \frac{1}{2h}C)u_{n-1} = F_n \qquad (3.24)$$

Newmark-β Method [27]

The central difference method discussed above is attractive in its simplicity in form and implementation. However, that the Central Difference Method is only conditionally stable. For this reason, many analysts prefer methods that are *unconditionally stable.* In this section we introduce the Newmark-β Method that is defined in terms of a single parameter that can be selected so that the specific method is indeed unconditionally stable.

The basis of the Newmark-β Method is the assumption that the system displacement vector u_{n+1} and its derivative $\dot{u}_{n+1}$ can be written in the form:

$$\dot{u}_{n+1} = \dot{u}_n + [(1-\gamma)\ddot{u}_n + \gamma\ddot{u}_{n+1}]h$$
$$u_{n+1} = u_n + \dot{u}_n h + [(1-2\beta)\ddot{u}_n + 2\beta\ddot{u}_{n+1}]\frac{h^2}{2} \qquad (3.25)$$

Each of these equations can be viewed as a type of generalized Taylor series approximation. The weighted average is a convex combination of approximate acceleration values. A conventional Taylor series approximation would result if the terms comprising the weighted average were simply replaced by the conventional term $\ddot{u}_n$.

The Newmark-β Method is an implicit method, with the discrete equation of motion

being enforced at the time step t_{n+1}. Thus, we require that:

$$M\ddot{u}_{n+1} + C\dot{u}_{n+1} + Ku_{n+1} = P_{n+1} = P(t_{n+1}) \qquad (3.26)$$

When the generalized derivative expressions, Eq.(3.25), are substituted into the discrete

equation of motion, Eq.(3.26), it is possible to organize terms and write a linear equation

for the new acceleration vector $\ddot{u}_{n+1}$. There are many possible organizations of the

calculations. It is also possible to frame the iterations in terms of u_{n+1}, to improve

efficiency.

Newmark originally proposed as an unconditionally stable scheme the Constant *Average*

Acceleration Method, in which case *β*=1/4 and *γ*=1/2.

3.2. Description of dynamic model

3.2.1. Introduction

In this thesis, the vehicle of the vehicle-bridge system model is modeled by rigid-body

dynamic method, which consists of a car body, two bogies, four wheel sets, and

suspensions [1, 28-31]. For bridge vibration, the rigid-body dynamic model is enough for

computing accuracy [32]. Dr. Yingjie Wang [33] established a 2D vehicle-bridge model

to study the vehicle-bridge dynamic responses with a flexible car body. Based on Wang's

model, the author improves the model to calculate the strain result from the analysis. The 2D vehicle-bridge model used in this thesis is shown in Figure 35.
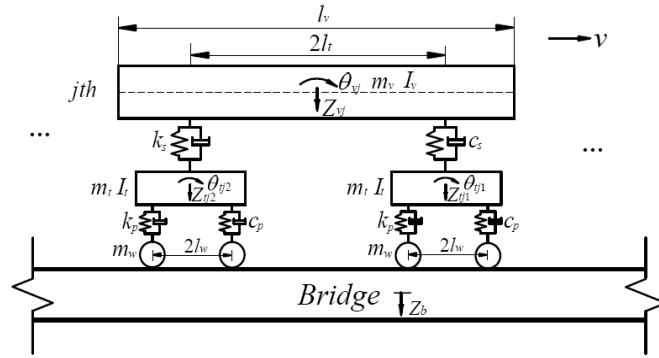
Figure 35. 2D Vehicle-bridge system model

As shown in Figure 35, the moving train running over a railway bridge is composed of several vehicles, and the simple bridge is modeled as a linear elastic Bernoulli-Euler beam with identical sections. The interaction responses of the train-bridge system will be computed using the modal superposition method along with Newmark-β method.

3.2.2. Vehicle model

In the vehicle model, the following assumptions are adopted for the vehicle model:

1. Each vehicle is composed of one car body, two identical bogies, and four identical wheel sets, and these components are regarded as rigid bodies and their elastic deformations are neglected.

2. The primary and secondary suspension systems are modeled as linear spring-dashpot units.

3. For each car body and bogie, there are two DOFs, designated by vertical displacement and rotation about the center point, as shown in Figure 36.

4. The four wheel sets of each vehicle are supposed to be in full contact with the bridge at all times and the motions of the wheel sets are linked to the movement of the bridge, so the independent DOFs of the vehicle system will be eliminated.
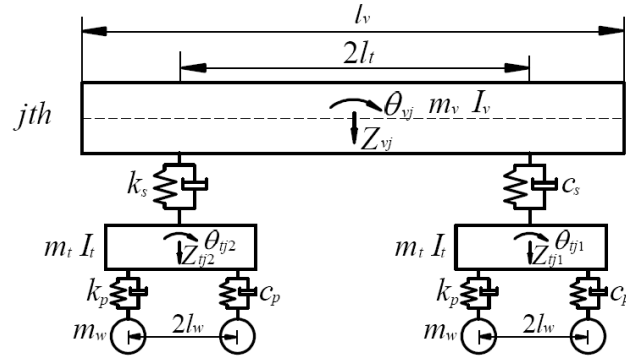
Figure 36. 2D Vehicle model

As shown in Figure 36, the notations of the components of the vehicle are defined in Table 4.

Table 4. Notations of vehicle model

Item	Notation
Mass of car body	m_v
Mass of bogie	m_t
Mass of wheel set	m_w
Mass moment of inertia of car body	I_v
Mass moment of inertia of bogie	I_t
Stiffness of primary suspension	k_p
Stiffness of secondary suspension	k_s
Damping of primary suspension	c_p
Damping of secondary suspension	c_s
Longitudinal distance of car body	l_v
Half of longitudinal distance between centers of gravity of front and rear bogies	l_t
Half of longitudinal distance between centers of gravity of wheel sets in each bogie	l_w

For the *jth* typical vehicle, the total degrees of freedom (DOFs) are 6, as shown in Table 5.

Table 5. DOFs of vehicle model

Components	vertical	roll
Car body	Z_{vj}	θ_{vj}
Front bogie (i=1)	Z_{tj1}	θ_{tj1}
Rear bogie (i=2)	Z_{tj2}	θ_{tj2}

3.2.3. Bridge model
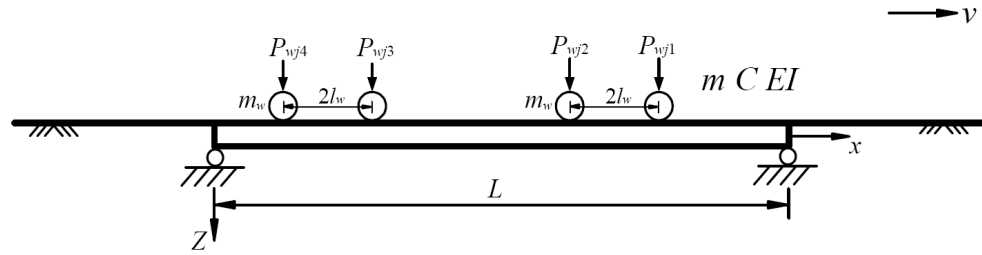
Figure 37. Simple bridge

As shown in Figure 37, the *jth* vehicle is moving on the simple bridge with length *L* at constant speed *v*. It is assumed that at the beginning the distance of the 1st vehicle to the left end of the bridge is x_0, and the location for each wheel set of the *jth* vehicle is x_{wjm} (m=1~4)

$$\begin{cases} x_{wj1}(t) = vt - x_0 - (j-1)l_v \\ x_{wj2}(t) = vt - x_0 - (j-1)l_v - 2l_w \\ x_{wj3}(t) = vt - x_0 - (j-1)l_v - 2l_t \\ x_{wj4}(t) = vt - x_0 - (j-1)l_v - 2(l_t + l_w) \end{cases} \tag{3.27}$$

Therefore, the equation of motion for the simple bridge subjected to moving vehicles can be written as:

$$EI\frac{\partial^4 Z(x,t)}{\partial x^4} + m\frac{\partial^2 Z(x,t)}{\partial t^2} + C\frac{\partial Z(x,t)}{\partial t} = F(x,t)$$

(3.28)

where, m is the mass per unit length of the bridge, C is the damping per unit length of the bridge, EI is the flexural rigidity of the bridge, and $F(x, t)$ is the external force acting on the bridge.

$$\begin{aligned}
F(x,t) = \sum_{j=1}^{N_v}\sum_{m=1}^{4}&\left\{\left[\left(\frac{m_v}{4}+\frac{m_t}{2}+m_w\right)g - m_w\ddot{Z}\left(x_{wjm},t\right)\right.\right.\\
&+c_p\left[\dot{Z}_{tjh}(t)+(-1)^{m-1}l_w\dot{\theta}_{tjh}(t)-\dot{Z}\left(x_{wjm},t\right)\right]\\
&\left.+k_p\left[Z_{tjh}(t)+(-1)^{m-1}l_w\theta_{tjh}(t)-Z\left(x_{wjm},t\right)\right]\right\}\\
&\cdot\delta\left(x-x_{wjm}\right)\cdot\left[H\left(t-t_{wjm}\right)-H\left(t-t_{wjm}-\Delta t\right)\right]
\end{aligned}$$

(3.29)

where j = 1, 2, 3, ..., N_vth vehicles on the bridge, $H(\cdot)$ is the unit step function to determine the axle is on the bridge or not, $\delta(\cdot)$ is Dirac's delta function, $Z(x,t)$ is the vertical displacement of the bridge, x_{wjm} is the position of the mth axle in the jth vehicle, t_{wjm} is the arriving time of the mth axle in the jth vehicle at the bridge, $\Delta t= L/v$ is the required time for the load to pass the bridge, and when m is 1 or 2, $h=1$ is the front bogie; m is 3 or 4, $h=2$ is the rear bogie.

3.2.4. Solution

Based on the modal superposition method, the displacement $Z(x,t)$ of the bridge can be expressed as

$$Z(x,t) = \sum_{n=1}^{\infty} q_n(t)\phi_n(x) \quad (n = 1,2\cdots\infty) \tag{3.30}$$

Where $q_n(t)$ is the generalized coordinate associated with the nth natural mode and $\Phi_n(x)$ is the nth mode shape function of the beam. The circular frequency and mode shape function of the simple bridge can be identified as:

$$\omega_n = \left(\frac{n\pi}{l}\right)^2 \sqrt{\frac{EI}{m}} \tag{3.31}$$

$$\phi_n(x) = \sin\left(\frac{n\pi x}{l}\right) \tag{3.32}$$

Substituting Eq.(3.30) and (3.29) into Eq.(3.28), multiplying by Φ_m and integrating the resultant equation with respect to x between 0 and L, and considering the orthogonality conditions of the natural vibration modes, the equation of motion of the nth generalized system in terms of the generalized displacement $q_n(t)$ is given as:

$$M_n\ddot{q}_n(t) + 2\xi_n\omega_n M_n\dot{q}_n(t) + K_n q_n(t) = F_n(t) \tag{3.33}$$

where ω_n, ξ_n and M_n are the modal frequency, damping ratio, and modal mass of the *nth*

mode, respectively, and $K_n \left(= M_n \omega_n^2\right)$ means the generalized stiffness of the *nth* mode.

The generalized force $F_n(t)$ is expressed as:

$$F_k(t) = \sum_{j=1}^{N_v} \sum_{m=1}^{4} \left\{ \left(\frac{m_v}{4} + \frac{m_t}{2} + m_w \right) g \phi_k\left(x_{wjm}\right) - m_w \sum_{n=1}^{NM_b} \ddot{q}_n(t) \phi_n\left(x_{wjm}\right) \phi_k\left(x_{wjm}\right) \right.$$

$$- \sum_{n=1}^{NM_b} \left[k_p q_n(t) + c_p \dot{q}_n(t) \right] \phi_n\left(x_{wjm}\right) \phi_k\left(x_{wjm}\right)$$

$$+ c_p \left[\dot{Z}_{tjh}(t) + (-1)^{m-1} l_w \dot{\theta}_{tjh}(t) \right] \phi_k\left(x_{wjm}\right) + k_p \left[Z_{tjh}(t) + (-1)^{m-1} l_w \theta_{tjh}(t) \right] \phi_k\left(x_{wjm}\right)$$

$$\left. - m_w \ddot{r}\left(x_{wjm}\right) \phi_k\left(x_{wjm}\right) \right\} \cdot \left[H\left(t - t_{wjm}\right) - H\left(t - t_{wjm} - \Delta t\right) \right] \tag{3.34}$$

Subsequently, substituting Eq.(3.34) into Eq.(3.33) and moving the terms with

$(q_i, \dot{q}_i, \ddot{q}_i, Z_k, \dot{Z}_k)$ to the left side of the differential equation, one can transform the

equation of motion for thesimple bridge coupled with moving vehicles into the following

generalized equation:

$$M_k \ddot{q}_k(t) + m_w \sum_{j=1}^{N_v} \sum_{m=1}^{4} \sum_{n=1}^{NM_b} \ddot{q}_n(t) \Phi_{nk} \tilde{H}_{wjm} + 2\xi_k \omega_k M_k \dot{q}_k(t)$$

$$+ c_p \sum_{j=1}^{N_v} \sum_{m=1}^{4} \sum_{n=1}^{NM_b} \dot{q}_n(t) \Phi_{nk} \tilde{H}_{wjm} + M_k \omega_k^2 q_k(t) + k_p \sum_{j=1}^{N_v} \sum_{m=1}^{4} \sum_{n=1}^{NM_b} q_n(t) \Phi_{nk} \tilde{H}_{wjm}$$

$$- c_p \sum_{j=1}^{N_v} \sum_{m=1}^{4} \dot{Z}_{tjh}(t) \Phi_k \tilde{H}_{wjm} - k_p \sum_{j=1}^{N_v} \sum_{m=1}^{4} Z_{tjh}(t) \Phi_k \tilde{H}_{wjm} \tag{3.35}$$

$$- (-1)^{m-1} c_p l_w \sum_{j=1}^{N_v} \sum_{m=1}^{4} \dot{\theta}_{tjh}(t) \Phi_k \tilde{H}_{wjm} - (-1)^{m-1} k_p l_w \sum_{j=1}^{N_v} \sum_{m=1}^{4} \theta_{tjh}(t) \Phi_k \tilde{H}_{wjm}$$

$$= \sum_{j=1}^{N_v} \sum_{m=1}^{4} \left(\frac{m_v}{4} + \frac{m_t}{2} + m_w \right) g \Phi_k \tilde{H}_{wjm}$$

where $\tilde{H}_{wjm} = H\left(t - t_{wjm}\right) - H\left(t - t_{wjm} - \Delta t\right)$, $\Phi_{nk} = \phi_n\left(x_{wjm}\right) \phi_k\left(x_{wjm}\right)$, $\Phi_k = \phi_k\left(x_{wjm}\right)$.

According to the motion equations of car body, the vertical and rotation equation motion of the car body can be written as:

$$m_v \ddot{Z}_{vj}(t) + k_s \left[2Z_{vj}(t) - Z_{tj1}(t) - Z_{tj2}(t) \right]$$
$$+ c_s \left[2\dot{Z}_{vj}(t) - \dot{Z}_{tj1}(t) - \dot{Z}_{tj2}(t) \right] = 0$$

(3.36)

$$I_v \ddot{\theta}_{vj}(t) + k_s l_t \left[2l_t \theta_{vj}(t) - Z_{tj1}(t) + Z_{tj2}(t) \right]$$
$$+ c_s l_t \left[2l_t \dot{\theta}_{vj}(t) - \dot{Z}_{tj1}(t) + \dot{Z}_{tj2}(t) \right] = 0$$

(3.37)

According to the motions equations of front bogie, the vertical and rotation equation motion of the front bogie can be written as:

$$m_t \ddot{Z}_{tj1}(t) + k_p \left[2Z_{tj1}(t) - \sum_{n=1}^{NM_b} q_n(t)\phi_n(x_{wj1}) - \sum_{n=1}^{NM_b} q_n(t)\phi_n(x_{wj2}) \right]$$
$$+ c_p \left[2\dot{Z}_{tj1}(t) - \sum_{n=1}^{NM_b} \dot{q}_n(t)\phi_n(x_{wj1}) - \sum_{n=1}^{NM_b} \dot{q}_n(t)\phi_n(x_{wj2}) \right]$$
$$- k_s \left[Z_{vj}(t) + l_t \theta_{vj}(t) - Z_{tj1}(t) \right] - c_s \left[\dot{Z}_{vj}(t) + l_t \dot{\theta}_{vj}(t) - \dot{Z}_{tj1}(t) \right] = 0$$

(3.38)

$$I_t \ddot{\theta}_{tj1}(t) + k_p l_w \left[2l_w \theta_{tj1}(t) - \sum_{n=1}^{NM_b} q_n(t)\phi_n(x_{wj1}) + \sum_{n=1}^{NM_b} q_n(t)\phi_n(x_{wj2}) \right]$$
$$+ c_p l_w \left[2l_w \dot{\theta}_{tj1}(t) - \sum_{n=1}^{NM_b} \dot{q}_n(t)\phi_n(x_{wj1}) + \sum_{n=1}^{NM_b} \dot{q}_n(t)\phi_n(x_{wj2}) \right] = 0$$

(3.39)

According to the motion equations of rear bogie, the vertical and rotation equation motion of the rear bogie can be written as:

$$m_t\ddot{Z}_{tj2}(t)+k_p\left[2Z_{tj2}(t)-\sum_{n=1}^{NM_b}q_n(t)\phi_n(x_{wj3})-\sum_{n=1}^{NM_b}q_n(t)\phi_n(x_{wj4})\right]$$

$$+c_p\left[2\dot{Z}_{tj2}(t)-\sum_{n=1}^{NM_b}\dot{q}_n(t)\phi_n(x_{wj3})-\sum_{n=1}^{NM_b}\dot{q}_n(t)\phi_n(x_{wj4})\right] \qquad (3.40)$$

$$-k_s\left[Z_{vj}(t)-l_t\theta_{vj}(t)-Z_{tj2}(t)\right]-c_s\left[\dot{Z}_{vj}(t)-l_t\dot{\theta}_{vj}(t)-\dot{Z}_{tj2}(t)\right]=0$$

$$I_t\ddot{\theta}_{tj2}(t)+k_pl_w\left[2l_w\theta_{tj2}(t)-\sum_{n=1}^{NM_b}q_n(t)\phi_n(x_{wj3})+\sum_{n=1}^{NM_b}q_n(t)\phi_n(x_{wj4})\right]$$

$$+c_pl_w\left[2l_w\dot{\theta}_{tj2}(t)-\sum_{n=1}^{NM_b}\dot{q}_n(t)\phi_n(x_{wj3})+\sum_{n=1}^{NM_b}\dot{q}_n(t)\phi_n(x_{wj4})\right]=0 \qquad (3.41)$$

As shown in Eq.(3.35) to (3.41), the simple bridge and the moving vehicles are coupled and interacting with each other. By combining Eq.(3.35) to (3.41), the equations of motion including the simple bridge and all of the vehicles in the modal space can be presented in a matrix form as:

$$[M]\{\ddot{U}\}+[C]\{\dot{U}\}+[K]\{U\}=\{F\} \qquad (3.42)$$

where $[M]$, $[C]$, $[K]$ denote the mass, damping and stiffness matrices; $(\{U\},\{\dot{U}\},\{\ddot{U}\})$ are the vectors of displacement, velocity, and acceleration, respectively; and $\{F\}$ represents the vector of exciting forces applied to the dynamic system.

To compute both the dynamic responses of the simple bridge and moving vehicles, the generalized matrix equation of motion given in Eq. (3.42) will be solved using a step-by-step integration method, i.e., the Newmark-β method. In this study, $\beta=1/4$ and $\gamma=1/2$ are selected, which implies a constant acceleration with unconditional numerical stability [27].

Chapter IV

Results from Analysis

4.1. Analysis results from field testing

From the field testing, the strain, velocity and deflection data was measured for the open deck steel bridges. In the following part, we will discuss the allowable stress and obtain the first natural bending frequency.

4.1.1. Natural frequency from field testing

Figure 38 shows the typical velocity response of girder in Raritan Valley Line MP 31.15. "Before" means the structural response before the train had traveled on the span and "After" means the structural response after that train had left the span, which also describes the free vibration of the bridge. By analyzing the data with Fast Fourier transform (FFT), the RT derived the velocity spectrum for "all" date and "after" data. Figure 39 through Figure 56 describe the velocity spectrum for different runs. Figure 39 shows the frequency domain result for "all" data in Run 9 for G8, the lower frequency component is the exciting train load while the component around 17 Hz is the first natural bending frequency. From the analysis, the exciting load frequency with maximum energy is 0.89 Hz. In run 9, the calculated main forced frequency is determined by speed over couple to couple length in Eq.(4.1), which is 0.83 Hz. Where v is the train speed and L is the couple to couple length of passenger train. The calculated forced frequency of the

train on the bridge is closed to the testing value. In Figure 40, the frequency domain of the "after" data was showed, the amplitude peak around 17.75 Hz is relatively high compared to concrete bridge [34]. From the analysis, we could tell the first natural frequency is 17.75 Hz for this case (Run 9, G8). The similar results were showed in the other cases (Figure 39 through Figure 56).

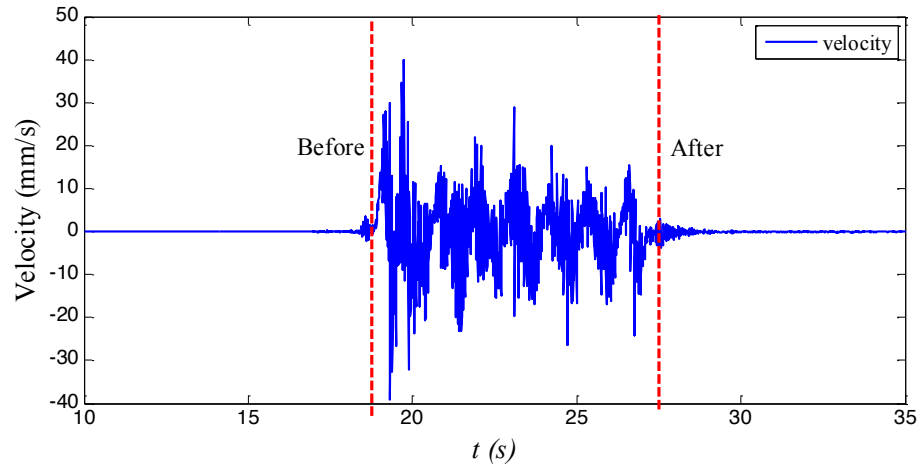$$Frequency = v/L = \frac{21.5m/s}{25.91m} = 0.83Hz \qquad (4.1)$$

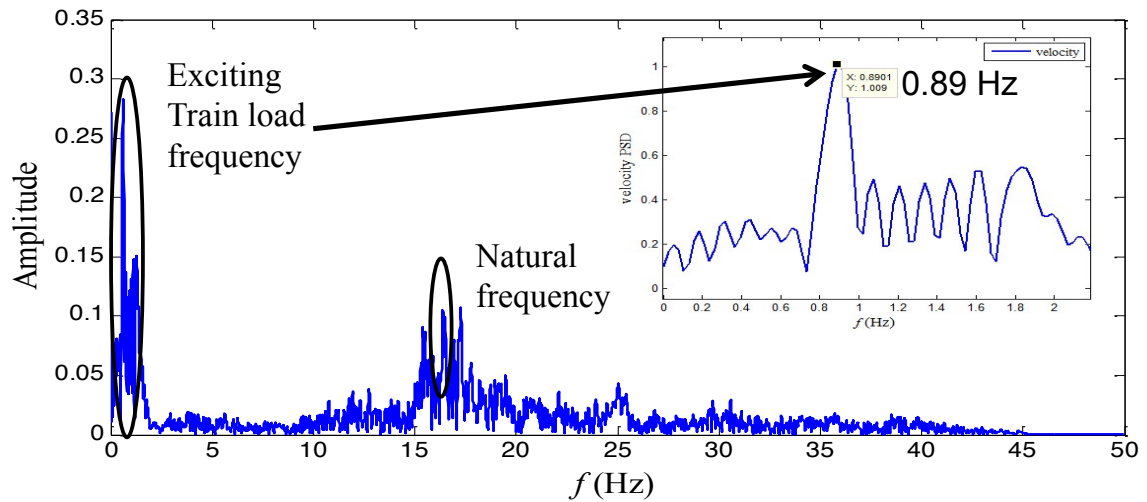Figure 38. Typical velocity response of girder

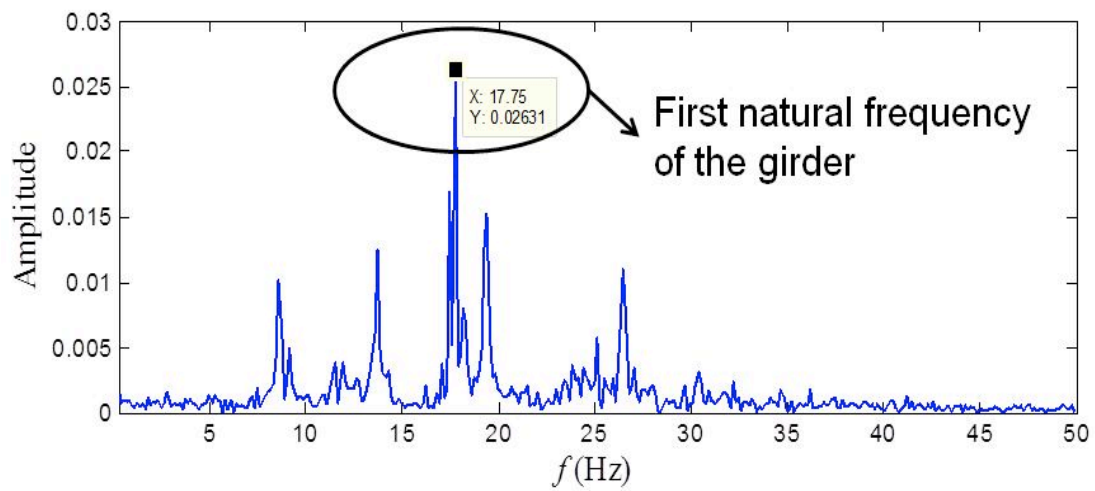Figure 39. Velocity spectrum (all data) for Run 9 (G8)

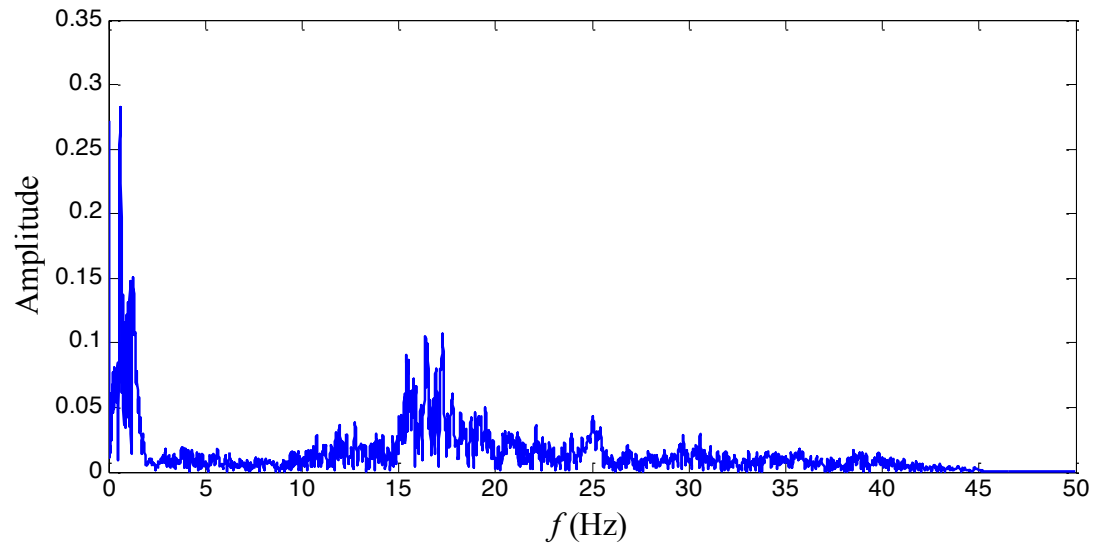Figure 40. Velocity spectrum (After) for Run 9 (G8)

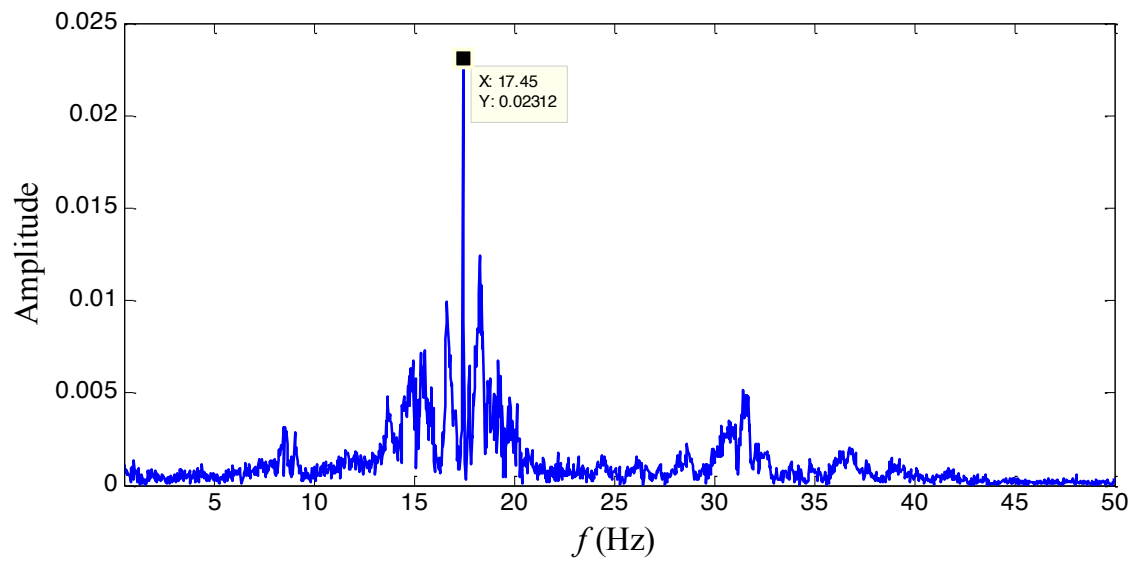Figure 41. Velocity spectrum (all data) for Run12 (G6)

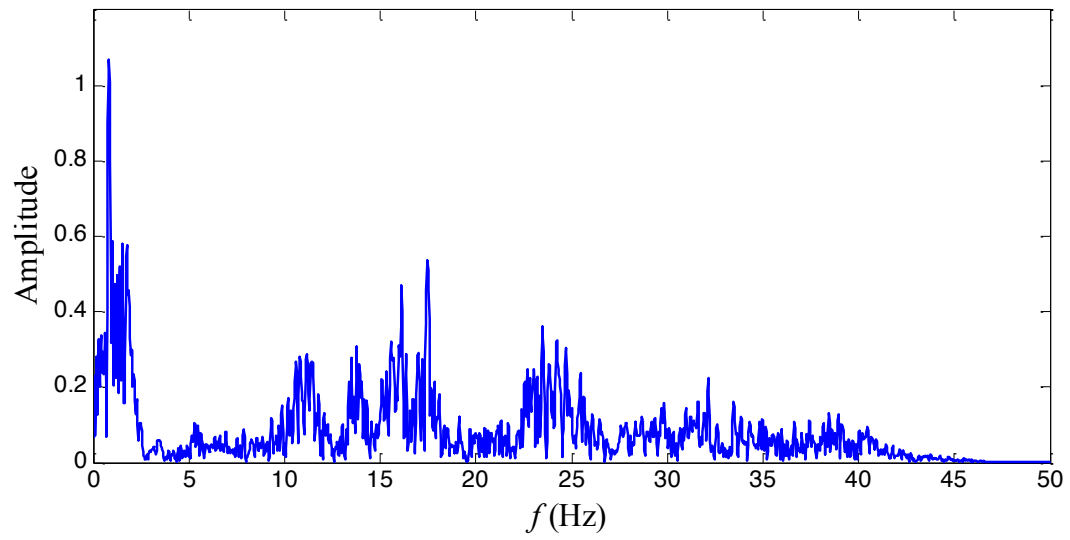Figure 42. Velocity spectrum (After) for Run12 (G6)

Figure 43. Velocity spectrum (all data) for Run13 (G8)

Figure 44. Velocity spectrum (After) for Run13 (G8)

Figure 45. Velocity spectrum (all data) for Run14 (G6)

Figure 46. Velocity spectrum (after) for Run14 (G6)

Figure 47. Velocity spectrum (all) for Run15 (G7)

Figure 48. Velocity spectrum (after) for Run15 (G7)

Figure 49. Velocity spectrum (all) for Run 17 (G7)

Figure 50. Velocity spectrum (after) for Run 17 (G7)
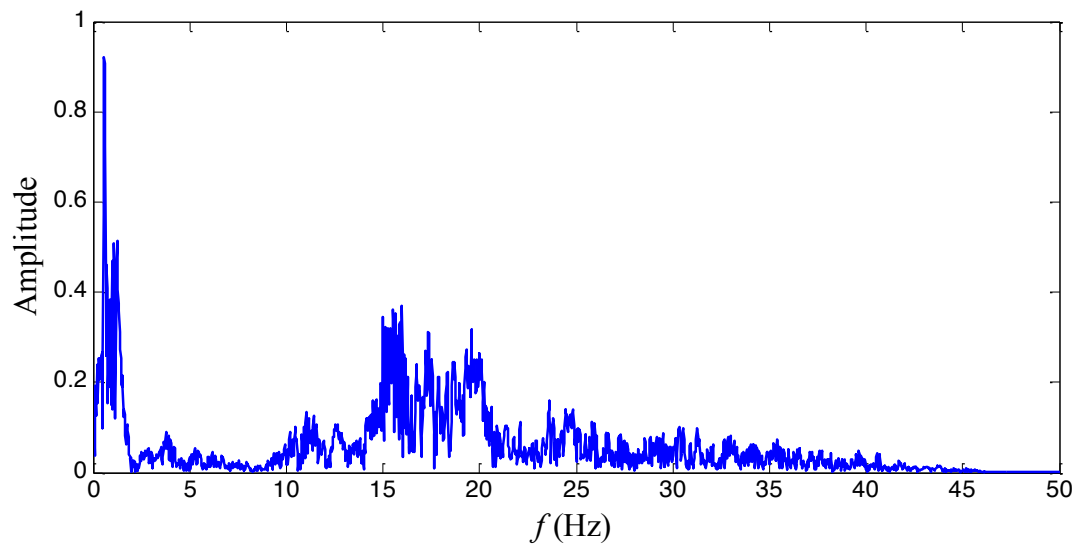
Figure 51. Velocity spectrum (all) for Run18 (G5)
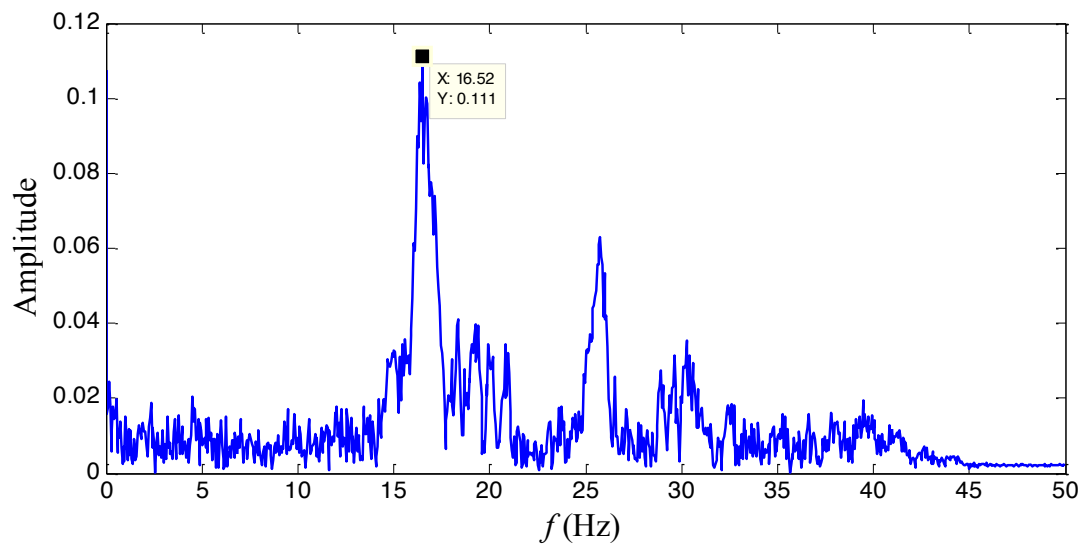
Figure 52. Velocity spectrum (after) for Run18 (G5)
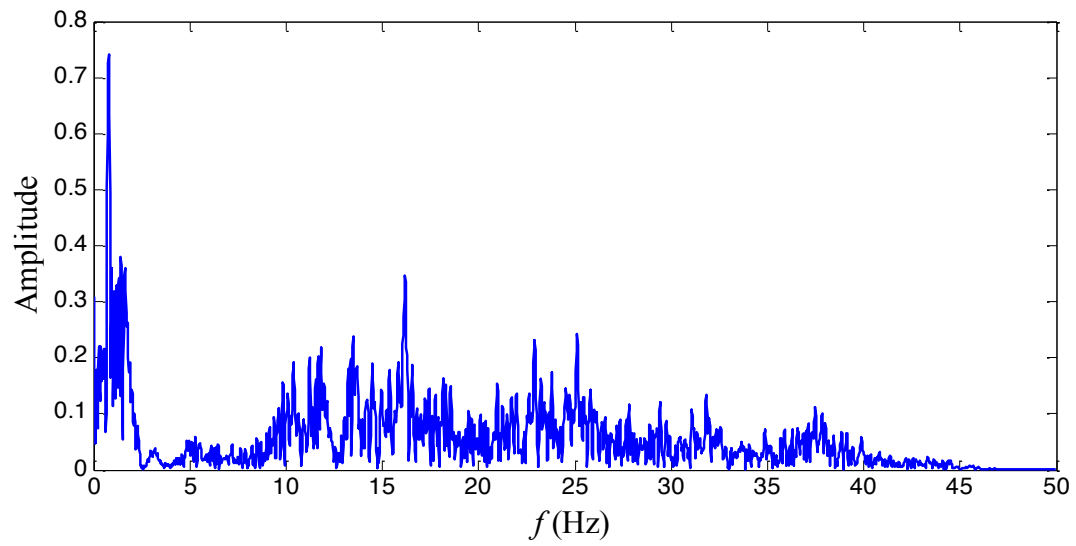
Figure 53. Velocity spectrum (all) for Run19 (G8)

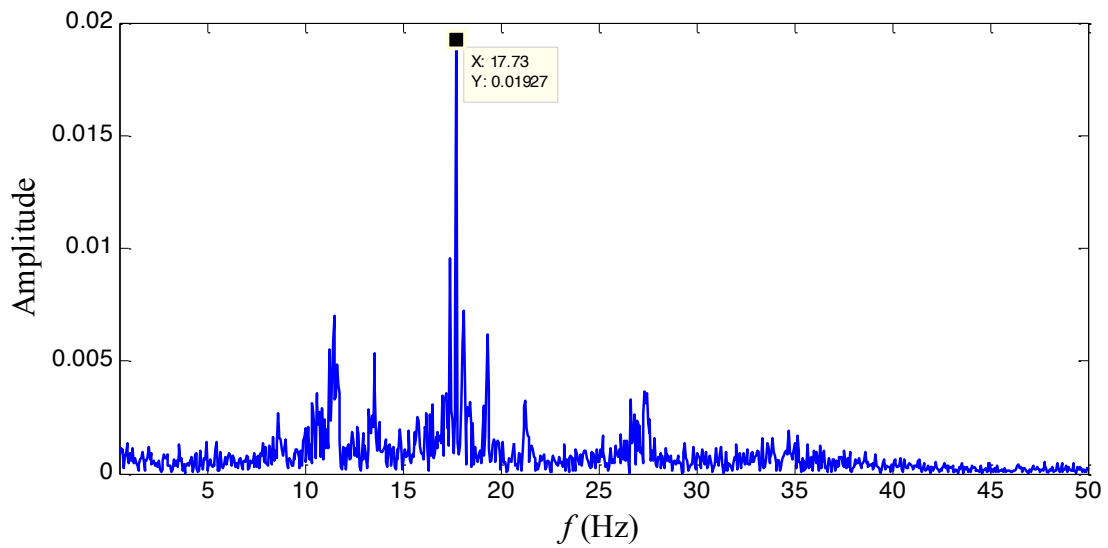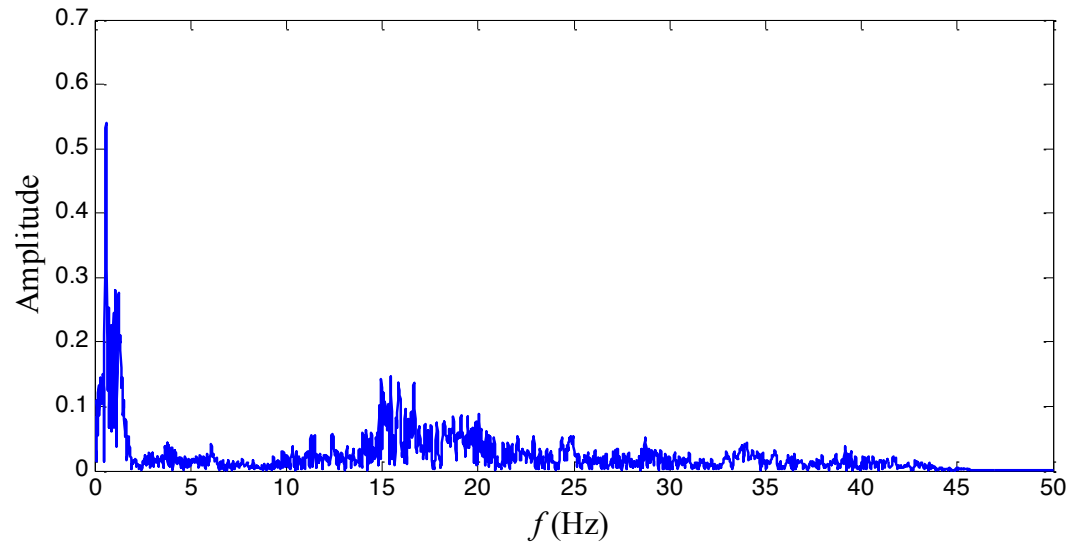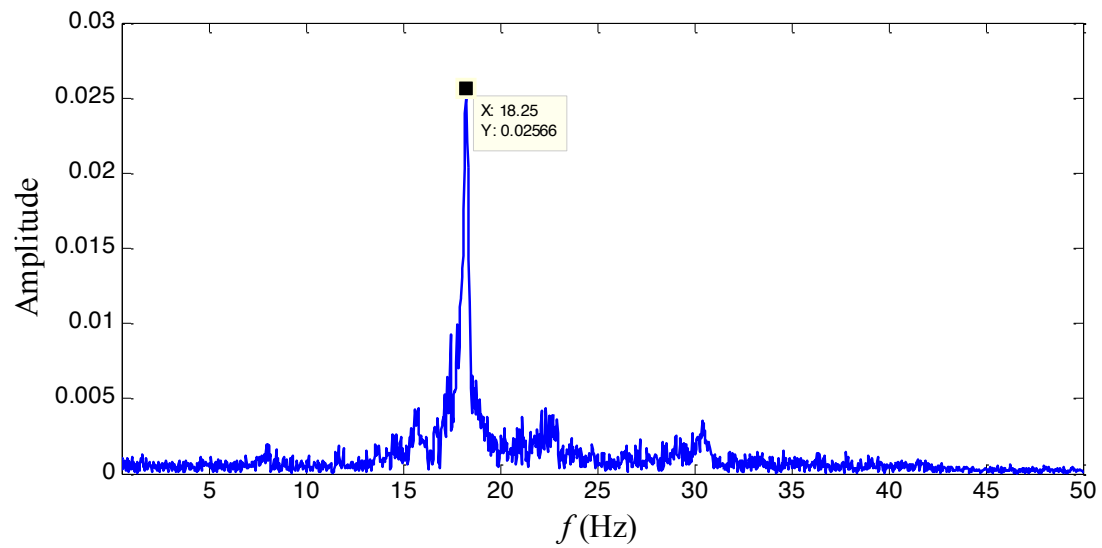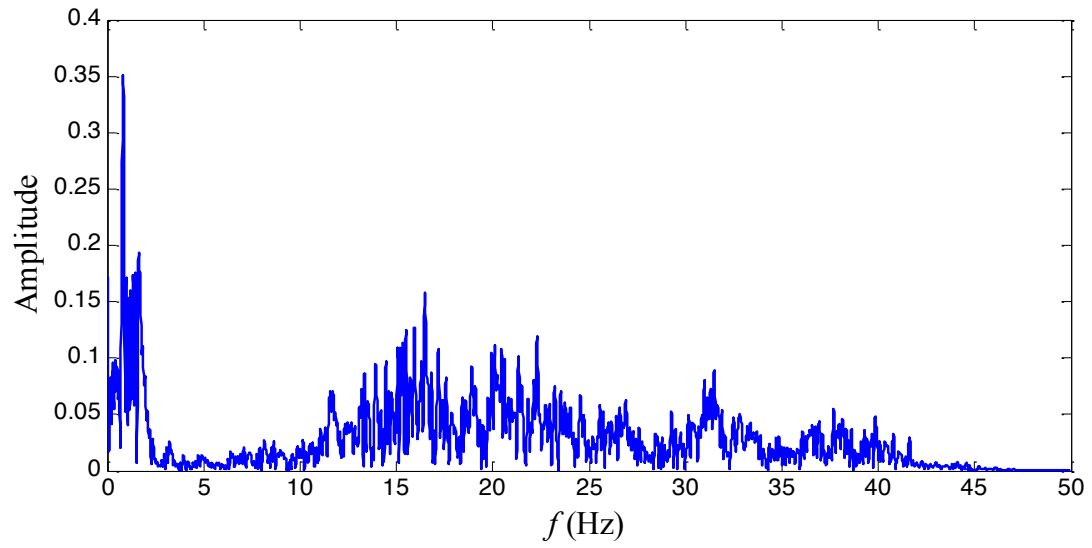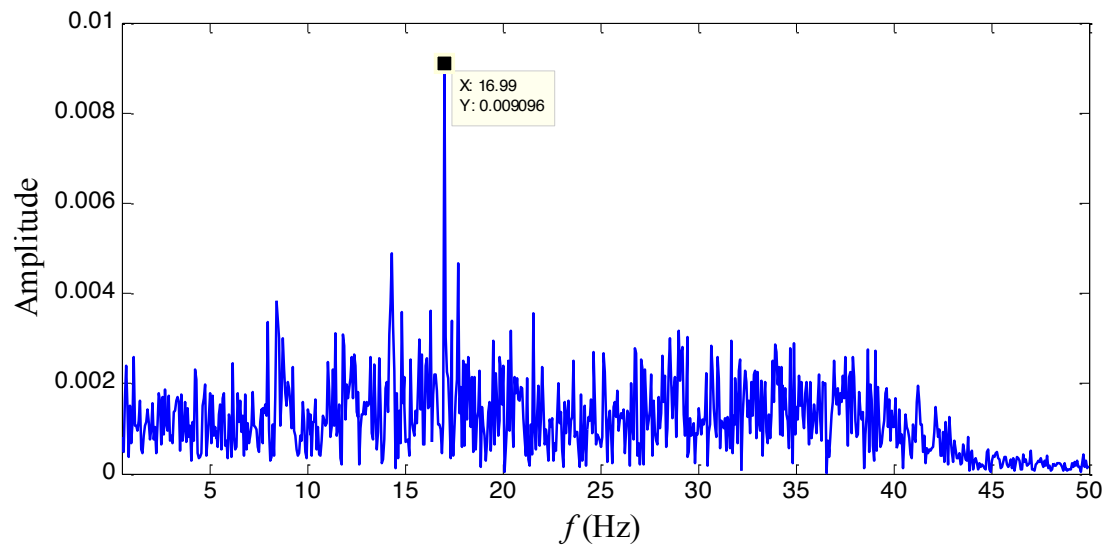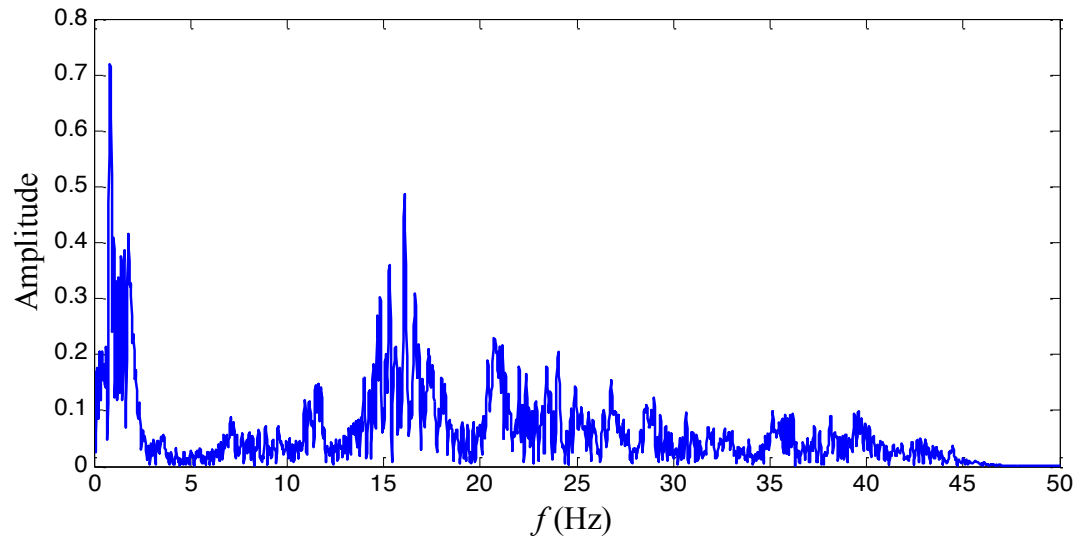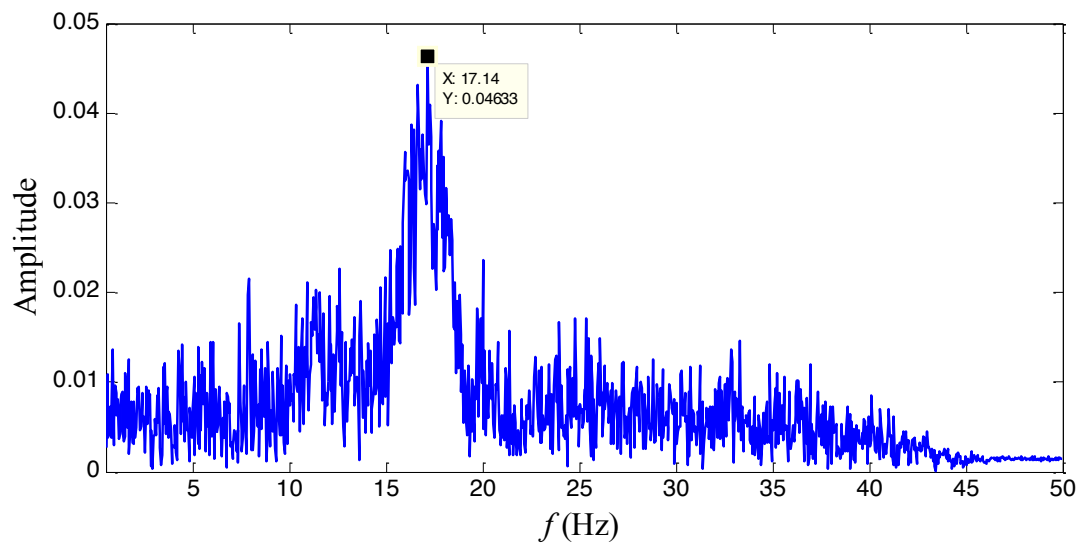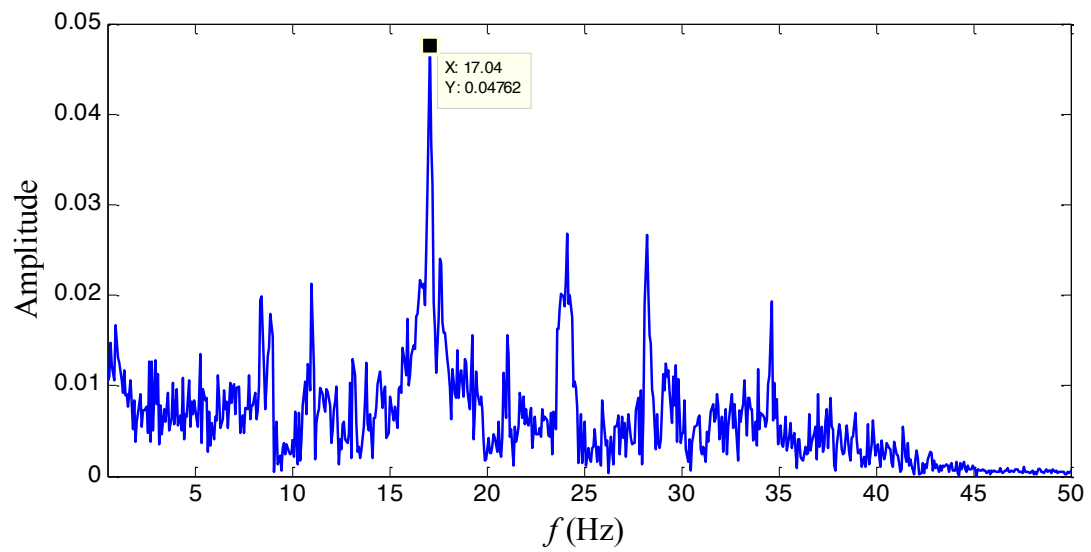

Figure 54. Velocity spectrum (after) for Run19 (G8)
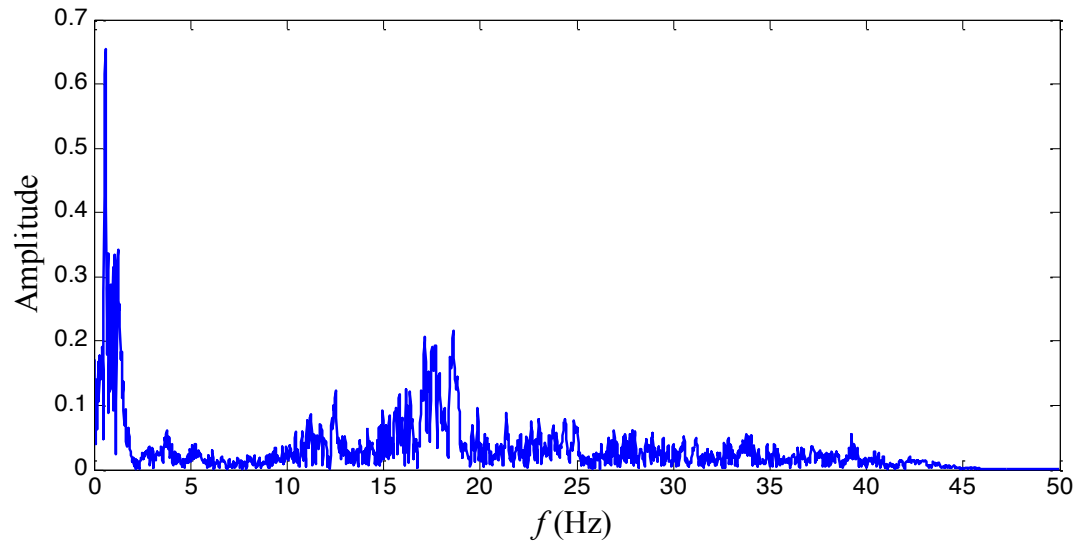
Figure 55. Velocity spectrum (all) for Run20 (G5)
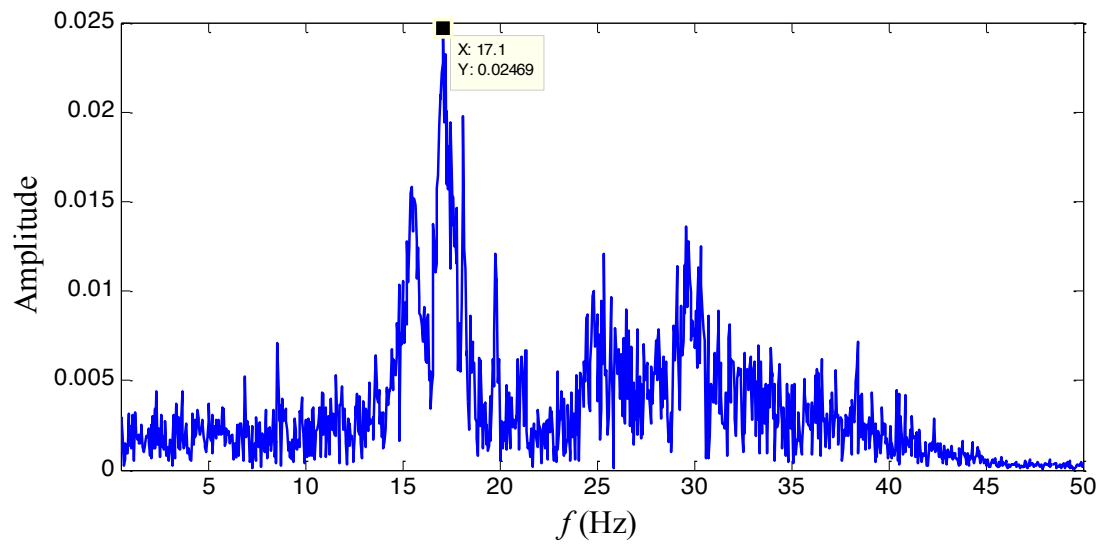
Figure 56. Velocity spectrum (after) for Run20 (G5)

Figure 57 shows the reflective tape location in the testing bridge. G5 and G6 are connected with the floor beam. Moreover, the section properties of G5 and G6 are the

same as-built from the inspection report. Theoretically, the first natural frequency gotten from the test data for G5 and G6 should be the close, similarly for G7 and G8.
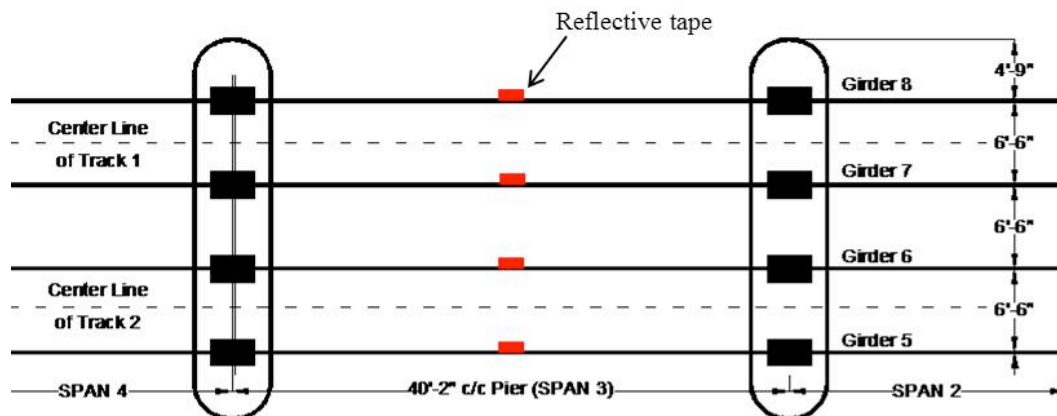
Figure 57. Location of reflective tape

Table 6 lists the summary of the testing results. For track 1, the first natural frequency of both G7 and G8 is between 17 Hz and 17.75 Hz. For Track 2, the first natural frequency varies from 16.52 Hz to 18.25 Hz. From the field-testing, considering the deviation during the testing, the first natural frequency for this span can be estimated as 17 Hz to 18 Hz.

Table 6. Summary of testing results

| Track # | Girder # | First Natural Frequency (Hz) | |
		First run	Second run
Track 1	G8	17.75	17.73
	G7	16.99	17.14
Track 2	G6	17.45	18.25
	G5	16.52	17.1

4.2. Analysis results from dynamic model

4.2.1. Natural frequency

For a simple supported beam, the natural frequency of the beam in the model is calculated as Eq.(4.2):

$$w = \left(\frac{n \times \pi}{l}\right)^2 \times \sqrt{\frac{EI}{m}}, \quad f = \frac{w}{2\pi} \tag{4.2}$$

Where l is the span length (ft) of the bridge, n is the mode number (1,2,…,n), EI is the bending stiffness (Nm^2) of the beam, m is the mass per unit length (kg/m) of the bridge.

From an engineering aspect, the first natural frequency is the major factor affecting the dynamic response of the bridge, consequently, in this part, only the first natural frequency was considered; therefore n is equal to one. From the cycle report, the Dead Load was taken as 0.531 k/ft, therefore, the equivalent mass of the bridge is m=2080kg/m. Substituting required information, the estimated first natural frequency is between 16.19 Hz and 22.11 Hz. Detail information is listed in Table 7. Based on the structural information, the approximate average bridge stiffness EI used in the model could be obtained as Eq.(4.3).

$$EI' = (EI_1 L_1 + EI_2 L_2 + EI_3 L_3)/(L_1 + L_2 + L_3) \tag{4.3}$$

Table 7. First natural frequency from model

L= 12.2 m	EI (Nm^2)	w (rad/s)	f (Hz)
m = 2080 kg/m	1.86E+09*	101.7	16.2
n = 1	3.46E+09**	138.9	22.1
	2.67E+09***	122	17.4

*Minimum EI is from section 1 (first cut off as-inspected)
**Maximum EI is from section 3 (mid-span as-built)
***Average EI is from calculation

4.2.2. Discussion for natural frequency of the bridge

Table 8 lists the comparison between hand calculation, field testing and FE model. The RT has also established 3-D FE model using commercial software Abaqus to help analysis in the part. The difference between FE model and testing data is 1.57 Hz to 2.33 Hz. During the field instrumentation and testing, the RT found several side stations (see Figure 58) at the mid-span of the testing span. This non-structural part could affect the natural frequency of the bridge but it is not noted and considered in the inspection report. Furthermore, it is hard to estimate the mass of the side station and not practical to consider this in the model. Therefore the omission of the side station could lead to the difference between the results from model and testing data. On the other hand, the uncertainty of testing, and the accuracy of the FE model could also affect the deviation between model and testing.

Table 8. Summary of different method estimating the first natural frequency

Methods	Frequency (Hz)
Dynamic model	17.4
Field testing data track 1	16.99-17.75
FE model	19.32

Figure 58. Side station connected at the mid-span of the testing span

4.2.3. Model validation

Time step

The time step is a very important parameter in obtaining accuracy in the solution. If a very small value of the time step is used, the solution will be more accurate. However this will increase the computational time. The time parameter selected has to be small enough to represent the reality but simultaneously large enough to not increase the computational

time extremely.

In order to analyze the model response with different time steps, the locomotive car PL-42 provided by NJ Transit is chosen. Three different time steps are considered: 0.01s, 0.001s and 0.0003s. In Figure 59, the maximum deflection under the passing train is depicted.

As shown in Figure 59 the higher time step selected, 0.01s does not provide an accurate solution, because this time step is not able to show the deflection peaks and it provides a solution with lower values than the rest of time steps selected. The other two time steps selected, 0.001s and 0.0003s give a very close solution, and the differences between both are negligible. Accordingly, to save computational time, in the rest of the sections, 0.001s was the time step used in the following discussion.
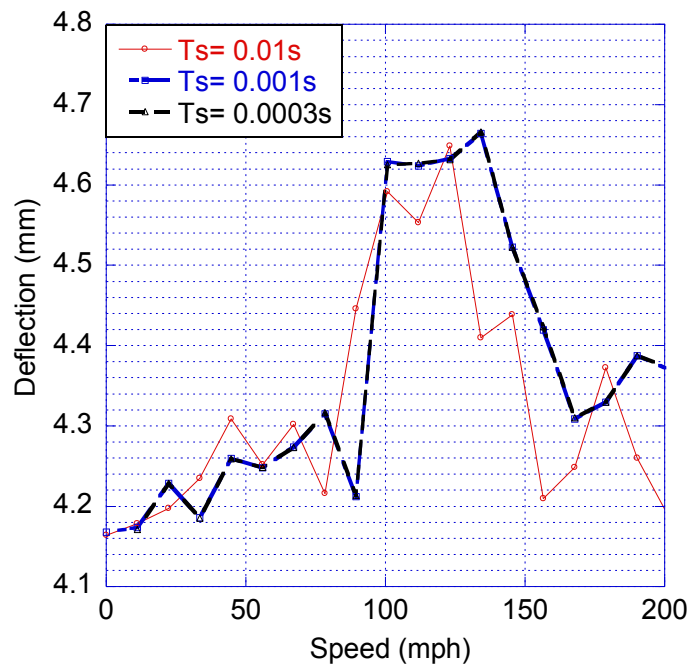
Figure 59. Deflection vs. train speed of PL-42 train with different steps

Verification of the convergence of the modes

In this dynamic model, we apply the modal superposition method to decrease the degree of freedoms to a limited number. The first consideration is the number of modes picked in the analysis. The selection of mode numbers affected not only the accuracy but also the computation time. According to related analysis in previous research, from the engineering point, the first several natural modes are of most importance. From Figure 60 it can be seen that the impact factor under various speeds remain the same when selecting 8 modes, 14 modes or 20 modes. To compute the deflection of the beam under traffic, 8 modes are enough to guarantee the accuracy of the analysis. However, compared to the deflection response, computation of the acceleration response always required consideration of an increased number of modes. Therefore, in this dynamic analysis, 20 modes were selected to conduct analysis in the following discussion. Please note, the damping ratio selected in this part $\zeta = 1.5\%$ for steel bridge.
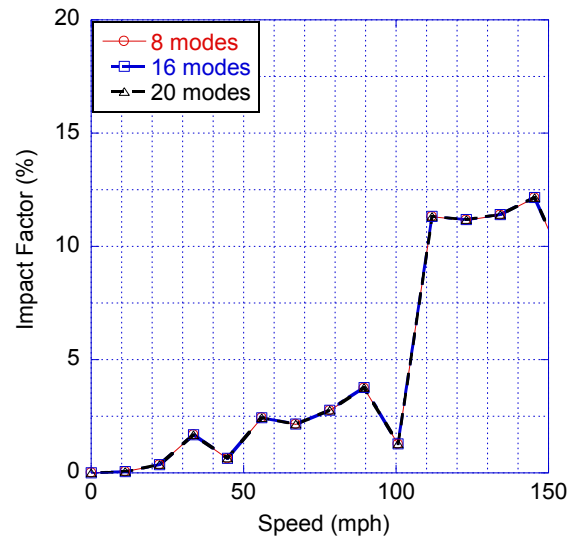
Figure 60. Impact factor vs. train speed with different number of modes of beam taken

into consideration

Damping ratio

The damping coefficient adopted to create the model is 1.5% according to the related

material for bridges with L<20 m and made up of steel sections. In this section, different

damping ratios were checked, specifically the following values; 1% and 2%. No

differences in the frequencies of the first ten bending and longitudinal modes of vibration

were found. Consequently, it can be concluded that the adoption of different damping

ratios does not affect the frequency values of the first ten bending and longitudinal modes

of vibration.

On the contrary, and as expected, the maximum deflection decreased as damping ratio

increased as depicted in Figure 61. Selecting a damping ratio of 2%, the maximum

impact factor is 14%, while impact factor is 13% when damping ratio is 1.5%, 12% when

1%. It can be concluded that the damping ratio does not greatly affect the impact factor.
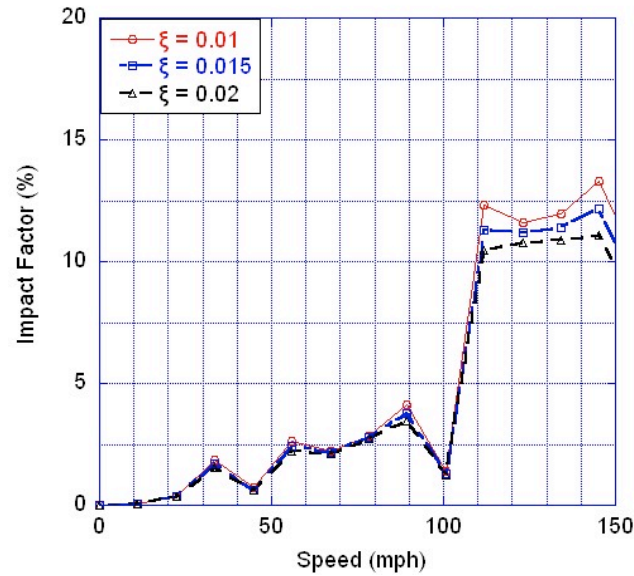
Figure 61. Impact factor vs. train speed with different damping ratios of the beam

In 2-D dynamic model, we cannot simulate the rocking effect when the train running through the bridge, so we consider 6 degree of freedoms of the train including: the vertical displacement and rotation along the center of the car body, the vertical displacement and rotation along the center of the front and rear bogie. The wheel set is assumed to be always in contact with the bridge so that the non-linear effect of the interaction of two subsystems was not included. In the model, one track of two integrating girders was incorporated into the beam model. Since the section properties are the same for all 4 girders under active track, the section modulus in the beam model would be double of the real girder property. In the model, the equivalent unit weight is transferred from the calculated dead load in [25].

Bridge model

In this dynamic model, the beam is established with uniform section property. Meanwhile, in the real life, the girder has 2 cut-offs that means the section property is varying along the length. Therefore, we need to validate the model with calculated stiffness EI value according to the first natural frequency obtained from the field testing. For the damping ratio, according to Kim [35], we can assume 0.015 for this non-ballast steel bridge. Span length and equivalent unit weight are taken from [25]. The summary of bridge information is listed below:

1. Bridge length L = 12.2 m

2. Calculated Stiffness EI = 2.67E9 N•m2

3. Equivalent unit weight = 1580 kg/m

4. Damping ratio=0.015 (Table 9)

Table 9. Results of the damping ratio [35]

Type	Maximum dynamic load (kN)	Number of data	Minimum damping ratio (%)	Maximum damping ratio (%)	Standard deviation	Average damping ratio (%)
Non- ballast	170	56	1.02	2.20	0.327	1.49
	220	52	0.92	2.09	0.241	1.23
Ballast track	170	46	0.94	2.42	0.246	1.40
	220	39	0.67	1.96	0.271	1.37
Concrete track	170	37	0.95	2.09	0.263	1.49
	220	33	1.27	1.86	0.161	1.56

Locomotive (PL-42) train model

Table 10 listed the parameter used in the dynamic model for locomotive car. For a locomotive car, the mass of bogie and wheel set is taken from [1], then the mass of car

body is computed by making the sum of car body, bogie and wheel set equal to the data provided by NJ Transit (288000 lbs for locomotive, 139000 lbs for passenger train). The dimension of the train model is also provided by NJ Transit. The mass moment of inertia, stiffness of suspension and damping of suspension is also taken from [1]. Similar information is also applied for passenger train.

Table 10. Parameters of locomotive

Item	Notation
Mass of car body	104324 kg
Mass of bogie	6080 kg **
Mass of wheel set	3560 kg **
Mass moment of inertia of car body	2080 t-m^2 **
Mass moment of inertia of bogie	3.93 t-m^2 **
Stiffness of primary suspension	1180 kN/m **
Stiffness of secondary suspension	530 kN/m **
Damping of primary suspension	39.2 kN-s/m **
Damping of secondary suspension	90.2 kN-s/m **
Longitudinal distance of car body	21.28 m *
Half of longitudinal distance between centers of gravity of front and rear bogies	6.605 m *
Half of longitudinal distance between centers of gravity of wheel sets in each bogie	1.45 m *

Passenger train model

Table 11 listed the parameter used in the dynamic model for passenger train. For the passenger train model, the mass of the bogie and wheel set is also taken from [1], and then the mass of car body is computed similar to locomotive car. The dimension of the train model is provided from NJ Transit. The mass moment of inertia, stiffness of suspension and damping of suspension is also taken from [1]. Similar information is also applied for passenger train.

Table 11. Parameters of passenger train

Item	Notation
Mass of car body	36804 kg
Mass of bogie	6080 kg **
Mass of wheel set	3560 kg **
Mass moment of inertia of car body	2080 t-m^2 **
Mass moment of inertia of bogie	3.93 t-m^2 **
Stiffness of primary suspension	1180 kN/m **
Stiffness of secondary suspension	530 kN/m **
Damping of primary suspension	39.2 kN-s/m **
Damping of secondary suspension	90.2 kN-s/m **
Longitudinal distance of car body	25.91 m *
Half of longitudinal distance between centers of gravity of front and rear bogies	9.07 m *
Half of longitudinal distance between centers of gravity of wheel sets in each bogie	1.30 m *

4.3. Comparison between testing and theoretical results

In this section, the collected strain, displacement and velocity data at mid-span of the bridge is compared with the results achieved from the dynamic model. Figure 62 to Figure 64 show the comparison of deflection, velocity and strain data at the mid-span point in the Raritan Valley Line Bridge. The results showed that the theoretical results agree with the field testing data very well. The difference between the theoretical and testing results is within 10% for strain. Figure 65 and Figure 66 showed the strain data comparison between theoretical and testing result at mid-span in Bergen County Line and North Jersey Coast Line, respectively. Both of the figures show good prediction by the dynamic model.
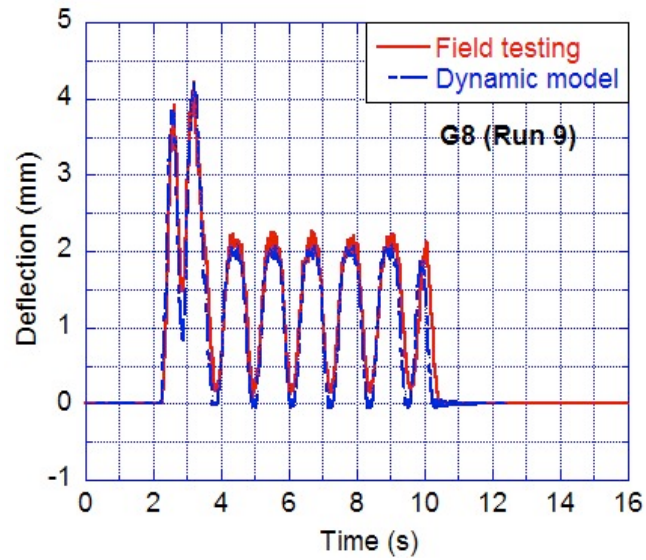
Figure 62. Displacement data comparison between field-testing data and model result
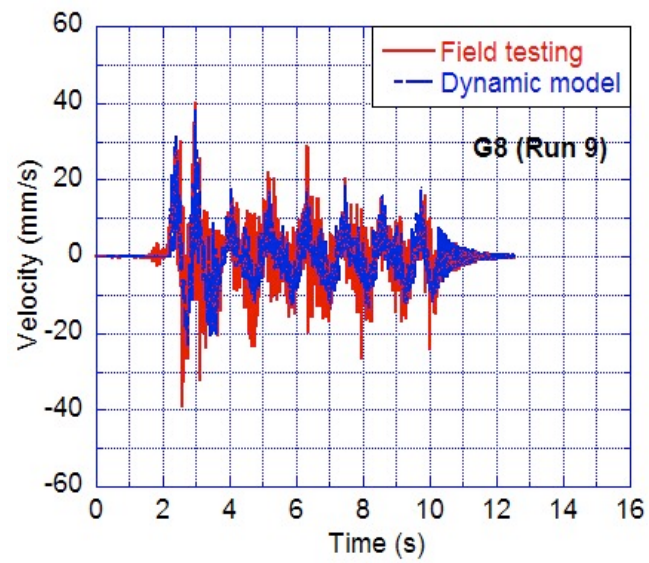

Figure 63. Velocity data comparison between field-testing data and model result
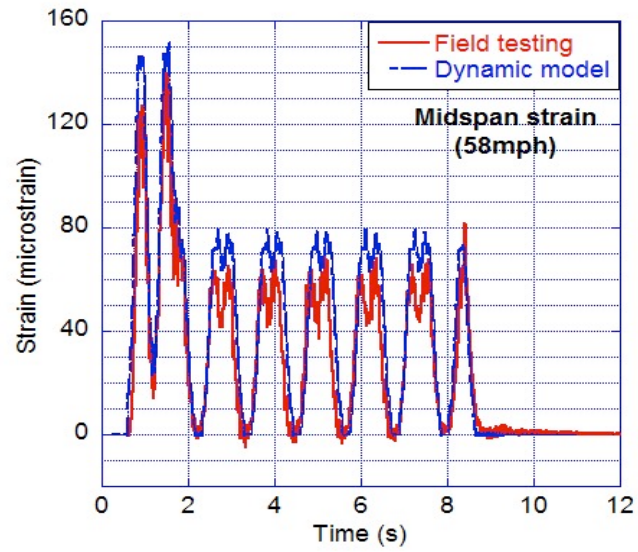
Figure 64. Strain data comparison between field-testing data and model result
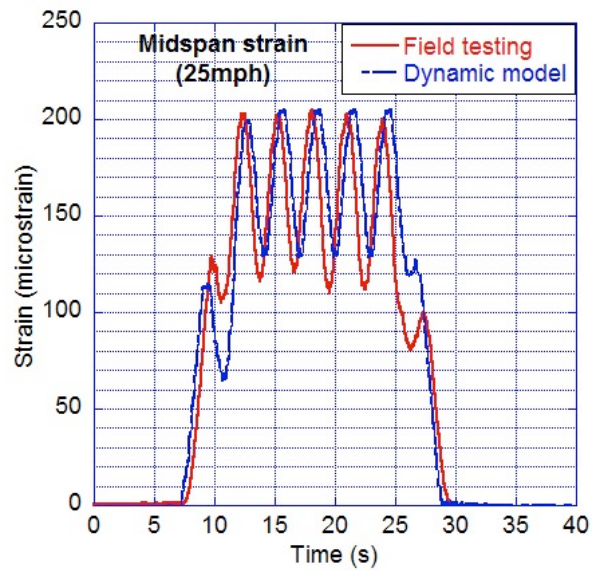
Figure 65. Strain data comparison between field-testing data and model result in Bergen

County Line Bridge
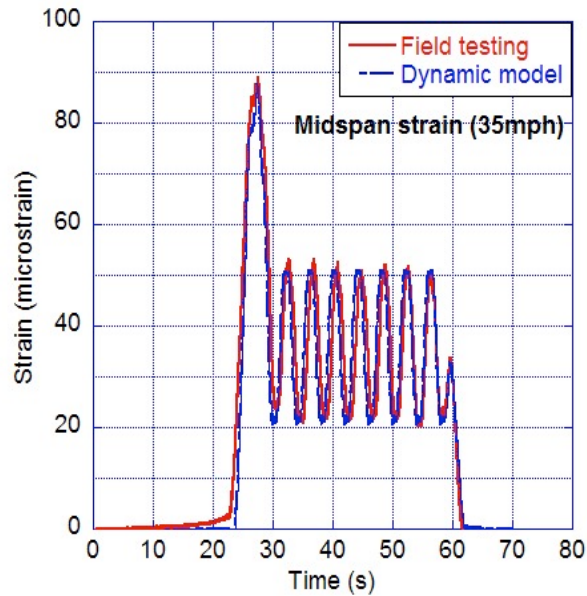
Figure 66. Strain data comparison between field-testing data and model result in North

Jersey Coast Line Bridge

4.4. Impact factor investigation

The study used results from three bridges for the analysis of impact factor. The following

sections summarize the results of the study.

4.4.1. Impact factor for three steel bridge and the critical speed

Natural frequency analysis was performed previously to determine the critical speed due

to successive passage of axle-loads. Some resonance phenomena may occur when

frequency of the passing axles is approximately equal to a modal frequency of the

structure because the trains have many axles as shown in Figure 25 to Figure 27. This

speed is calculated by Eq.(4.4) in [36]:

$$V_{cr} = f_1 \times S_{eff} \qquad\qquad (4.4)$$

where V_{cr}, is critical speed of train (m/s);f_1, is first-mode flexural frequency of bridge (Hz); S_{eff}, is axle spacing of train (m).

The critical speeds estimated for the different train types are given in Table 12. The results show that resonance can occur in three bridges within the typical operating speed range (150 mph). Referring to Figure 25 through Figure 27, six different axle spacings were considered in Table 12. The speed results in yellow are the reasonable resonance speed below 120 mph in Table 12. In order to verify the critical speed with the analysis results, the impact factor for the three steel bridges in Figure 67, Figure 68 and Figure 69, respectively, was listed.

For instance in Bergen County Line Bridge, it can be seen that the critical speed is 46 mph, 68 mph and 107 mph. Compared to the impact factor plot shown in Figure 68, we have the peak value at speeds around 47 mph, 70 mph and 100 mph. Similarly, in North Jersey Coast line Bridge, the critical speeds are 46 mph, 70 mph, and 103 mph.

Table 12. Critical speeds estimated for different train types.

Bridge Id.	Span length (m)	Frequency (Hz)	Critical speed (mile per hour)			Train type
Raritan	12.2	17.7	S_{eff}(m) = 2.6	S_{eff} (m) = 5.17	S_{eff} (m) = 7.77	Passenger train
			102.9	204.7	307.6	
			S_{eff} (m) = 15.54	S_{eff} (m) = 18.14	S_{eff} (m) = 25.91	
			615.3	718.2	1025.9	
Bergen	17.5	11.6	S_{eff} (m) = 1.778	S_{eff} (m) = 2.362	S_{eff} (m) = 4.14	AREMA 286 rail car
			46.1	61.3	107.4	
			S_{eff} (m) = 7.822	S_{eff} (m) = 9.6	S_{eff} (m) = 11.378	
			203	249.1	295.2	
Coast	25.9	7.8	S_{eff} (m) = 2.6	S_{eff} (m) = 5.17	S_{eff} (m) = 7.77	Passenger train
			45.4	90.2	135.6	
			S_{eff} (m) = 15.54	S_{eff}(m) = 18.14	S_{eff} (m) = 25.91	
			271.1	316.5	452.1	
Raritan	12.2	17.7	S_{eff} (m) = 2.89	S_{eff} (m) = 5.17	S_{eff} (m) = 10.3	PL-42 locomotive
			114.4	204.7	407.8	
			S_{eff}m) = 13.13	S_{eff} (m) = 16.08	S_{eff} (m) = 21.26	
			519.9	636.7	841.8	
Coast	25.9	7.8	S_{eff} (m) = 2.64	S_{eff} (m) = 5.91	S_{eff} (m) = 8.55	ALP-46a
			46.1	103.1	149.2	
			S_{eff} (m) = 8.3	S_{eff} (m) = 10.94	S_{eff} (m) = 13.58	
			144.8	190.9	236.9	

From the results, it can be seen that the axle spacing is an important factor that could affect the critical speed and the impact factor. The Impact factor has higher value when the train is running at critical speed. This is the so-called resonance phenomenon with regard to the train length other than the axle spacing.
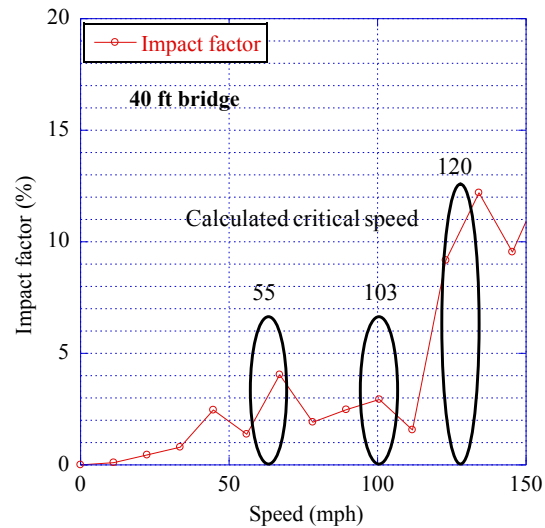

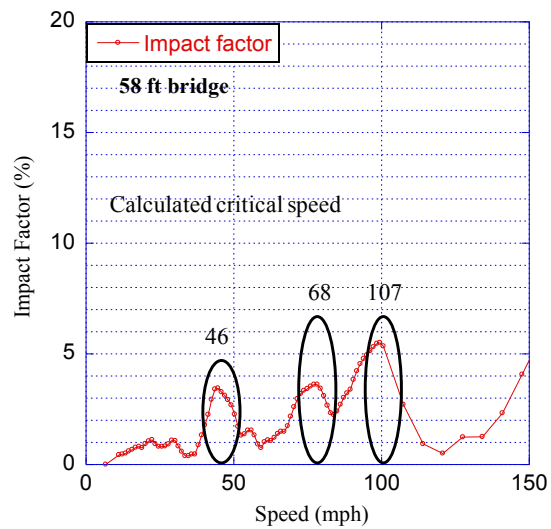Figure 67. Impact factor for Raritan Valley Line Bridge

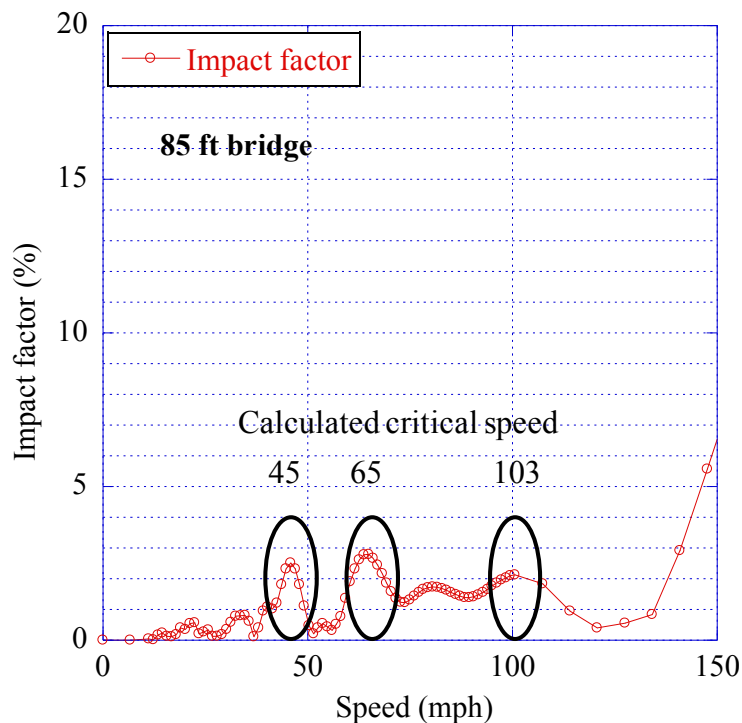Figure 68. Impact factor for Bergen County Line Bridge

Figure 69. Impact factor for North Jersey Coast Line Bridge

4.4.2. Impact factor comparison with AREMA Specifications

After obtaining the impact for each bridge, we could compare them with the AREMA specifications in the following figures (Figure 70, Figure 71, and Figure 72) with respect to speed or span length. From the comparison, we could conclude that the AREMA Specifications is relatively high at lower speed (under 100 mph). From Figure 71, the increased axle load has great effect affect the dynamic stress or strain however it does not affect the impact factor significantly from. The impact is very low at low speed compared to AREMA.

In Figure 73, the impact factor with respect to the bridge span length is listed. The result shows that impact factor decreased as the span length increases which agrees with the AREMA Specifications.

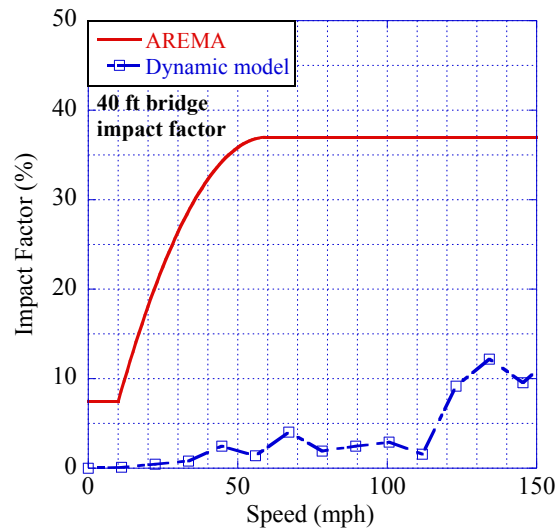

Figure 70. Impact factor comparison with AREMA Specifications for Raritan Valley
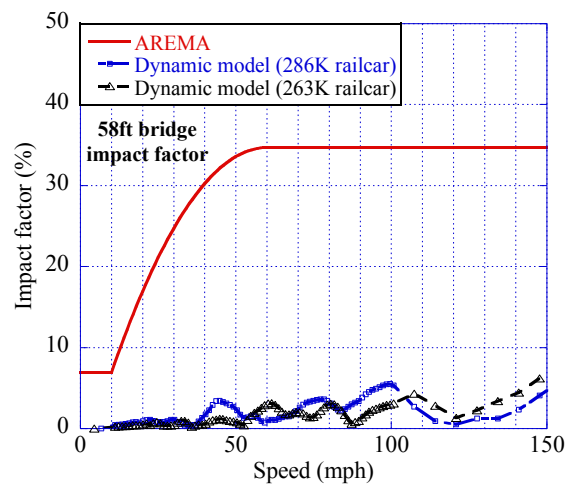
Line Bridge

Figure 71. Impact factor comparison with AREMA Specifications for Bergen County
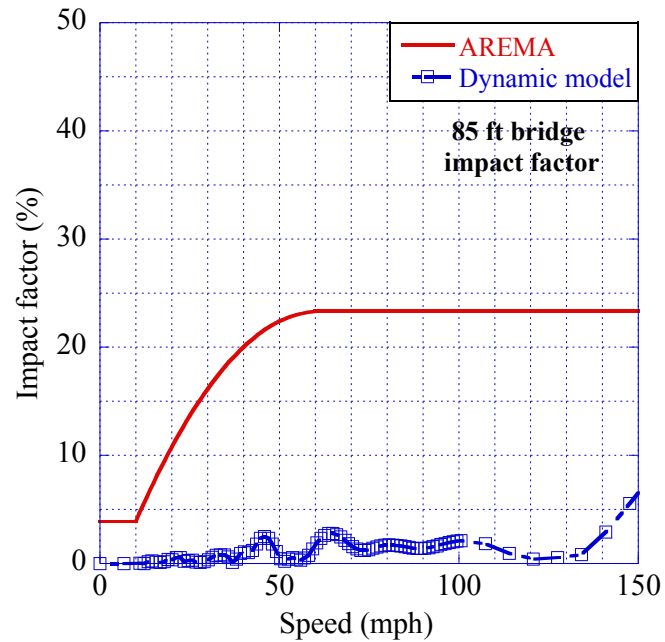
Line Bridge

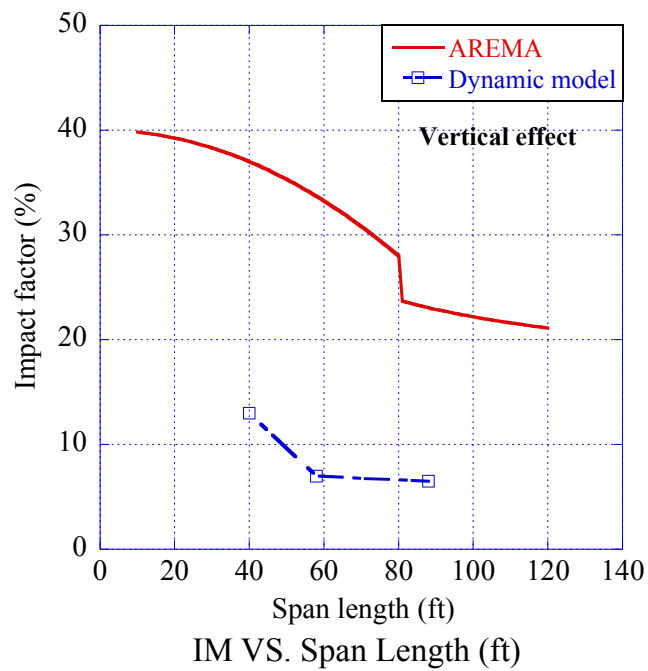Figure 72. Impact factor comparison with AREMA Specifications for North Jersey Coast

Line Bridge

IM VS. Span Length (ft)

Figure 73. Impact factor with respect to span length with AREMA Specifications

Chapter V

Conclusions and Future Research

5.1. Conclusion

In this thesis, a two-dimensional dynamic model of simply supported span steel bridges has been developed to successfully determine the impact factor as well as the overall dynamic behavior of the railroad bridges. Field instrumentation and testing of strain, displacement, and velocity were performed in order to compare results with those from the two dimensional dynamic model. Based on the results of this study, the following conclusions can be drawn:

- Since the unit mass of the steel bridge is low compared to concrete bridges, the first natural frequency is high.
- Axle spacing is an important factor that affects the critical speed and impact factor.
- Vehicle load have great effect on dynamic stress (strain) however it does not affect the impact factor significantly.
- The impact factor will slightly decrease as the damping ratios increases.
- The impact factor at a typical speed of 60 mph decreases as the span length increases as per AREMA.

- Impact factor decreases as the span length increases, which agrees with the AREMA code.

- AREMA is more conservative than the analysis results for train speeds less than 60 mph.

5.2. Suggestion for further work

The next step to help develop this work would be to create a 3D dynamic model using Matlab, which considers the rocking effect of the train to the bridge. Also, in addition to the flexural mode, the torsional modes need to be considered.

Rail roughness condition is a very important factor in evaluating impact factor and should also be considered in future dynamic models.

For steel bridges, it is also important to determine the impact factor for fatigue.

Reference

1. Yang, Y.B., J.D. Yau, and Y.S. Wu, *Vehicle-bridge interaction dynamics: with applications to high-speed railways,* 2004: World Scientific.

2. Willis., R., *Appendix to the report of the commissioners appointed to inquire into the application of iron to railway structures*, 1849.

3. LÓPEZ, J.M.E., *Traffic-induced vibrations on a two span composite railway bridge: Comparison of theory and measurements*, 2011, KTH Royal Institute of Technology: Stockholm.

4. GG., S., *Discussion of a differential equation relating to the breaking of railway bridges,* 1849: Trans Cambridge Philos Soc.

5. Michaltsos, G.T. and I.G. Raftoyiannis, *The influence of a train's critical speed and rail discontinuity on the dynamic behavior of single-span steel bridges.* Engineering Structures, 2010. 32(2): p. 570-579.

6. TIMOSHENKO, S., *Vibration problems in engineering,* 1937.

7. Inglis, S.C.E., *A mathematical treatise on vibrations in railway bridges,* 1934: University Press.

8. Fryba, L., *Vibration of solids and structures under moving loads,* 1999: Thomas Telford.

9. Fryba, L., *A rough assessment of railway bridges for high speed trains.* Engineering Structures, 2001. 23(5): p. 548-556.

10. D214, U.-E.C., *Report 9. Part A: Synthesis of the results of D214 research. Part B: Proposed UIC Leaflet*, 1999.

11. Xia, H., et al., *Experimental analysis of a high-speed railway bridge under Thalys trains.* Journal of Sound and Vibration, 2003. 268(1): p. 103-113.

12. Xia, H., et al., *Dynamic interaction analysis of a LIM train and elevated bridge system.* Journal of Mechanical Science and Technology, 2009. 23(12): p. 3257-3270.

13. Xia, H., et al., *Dynamic analysis of train-bridge system and its application in steel girder reinforcement.* Computers & Structures, 2001. 79(20-21): p. 1851-1860.

14. Xia, H. and N. Zhang, *Dynamic analysis of railway bridge under high-speed trains.* Computers & Structures, 2005. 83(23-24): p. 1891-1901.

15. Xia, H., N. Zhang, and G. De Roeck, *Dynamic analysis of high speed railway bridge under articulated trains.* Computers & Structures, 2003. 81(26-27): p. 2467-2478.

16. Xia, H., et al., *Dynamic analysis of a train-bridge system under wind action.* Computers & Structures, 2008. 86(19-20): p. 1845-1855.

17. Xia, H., N. Zhang, and W.W. Guo, *Analysis of resonance mechanism and conditions of train-bridge system.* Journal of Sound and Vibration, 2006. 297(3-5): p. 810-822.

18. Moghimi, H. and H.R. Ronagh, *Impact factors for a composite steel ebridge using non-linear dynamic simulation.* International Journal of Impact Engineering, 2008. 35(11): p. 1228-1243.

19. *AASHTO Manual,* 1998: American Association of State Highway and Transportation Officials

20. *AREMA Manual,* 2006: American Railway Engineering and Maintenance-of-Way Association.

21. Colin O'Connor and P.A. Shaw, *Bridge loads: an international perspective,* 2000: SPON Press.

22. *Ontario Highway Bridge design code (OHBD),* 1983: Downsview, Ontario, Canada: Ministry of Transportation.

23. *Bridge Design Code,* 1992: Australia's national road authority (AUST- ROADS), Sydney, Australia.

24. Hamidi, S.A. and F. Danshjoo, *Determination of impact factor for steel railway bridges considering simultaneous effects of vehicle speed and axle distance to span length ratio.* Engineering Structures, 2010. 32(5): p. 1369-1376.

25. Chas. H. Sells, I., *RIDGE INSPECTION SURVEY REPORT: RARITAN VALLEY LINE MP 31.15 OVER MIDDLE BROOK, FOURTH CYCLE,* 2007.

26. Bathe, K.J., *Finite Elements Procedure in Engineering Analysis,* 1982: Prentice Hall, Englewood Cliffs.

27. Newmark, N.M., *A Method of Computation for Structural Dynamics*, 1959: United States. p. 30p.

28. L, F., *Dynamics of railway bridges,* 1996: London: Thomas Telford.

29. Wu, Y.S. and Y.B. Yang, *Steady-state response and riding comfort of trains moving over a series of simply supported bridges.* Engineering Structures, 2003. 25(2): p. 251-265.

30. Zhang, N., et al., *A VEHICLE-BRIDGE LINEAR INTERACTION MODEL AND ITS VALIDATION.* International Journal of Structural Stability and Dynamics, 2010. 10(2): p. 335-361.

31. Lou, P., *Finite element analysis for train-track-bridge interaction system.* Archive of Applied Mechanics, 2007. 77(10): p. 707-728.

32. Cheng, Y.S., F.T.K. Au, and Y.K. Cheung, *Vibration of railway bridges under a moving train by using bridge-track-vehicle element.* Engineering Structures, 2001. 23(12): p. 1597-1606.

33.   Wang, Y., *Study on Vehicle-Bridge Dynamic Responses with Flexible Carbody and Riding Comfort Evaluation*, 2011, Beijing Jiaotong University: Bejing, China.

34.   Huang, D.Z., *Dynamic and Impact Behavior of Half-Through Arch Bridges.* Journal of Bridge Engineering, 2005. 10(2): p. 133-141.

35.   Kim, S.I., *Experimental evaluations of track structure effects on dynamic properties of railway bridges.* Journal of Vibration and Control, 2011. 17(12): p. 1817-1826.

36.   Lee, H.-H., J.-C. Jeon, and K.-S. Kyung, *Determination of a reasonable impact factor for fatigue investigation of simple steel plate girder railway bridges.* Engineering Structures, 2012. 36: p. 316-324.